Fucoidan Prolongs the Circulation Time of Dextran-Coated Iron Oxide Nanoparticles

Maha R. A. Abdollah[§1,2] & Thomas J. Carter[§1], Clare Jones[3], Tammy L. Kalber[4], Vineeth Rajkumar[1], Berend Tolner[1], Cordula Gruettner[5], May Zaw-Thin[4], Julia Baguña Torres[3], Matthew Ellis[6], Mathew Robson[1], R. Barbara Pedley[1], Paul Mulholland[1], Rafael T. M. de Rosales[§3] and Kerry Ann Chester[§1]*

[1] UCL Cancer Institute, University College London (UCL), Paul O'Gorman Building, 72 Huntley Street, London, UK.

[2] Department of Pharmacology and Biochemistry, Faculty of Pharmacy, The British University in Egypt (BUE), El Shorouk City, Misr- Ismalia Desert Road, Cairo, Egypt.

[3] School of Biomedical Engineering & Imaging Sciences, King's College London (KCL), St Thomas' Hospital, London, UK.

[4] Centre for Advanced Biomedical Imaging, Division of Medicine and Institute of Child Health, University College London, London, UK.

[5] Micromod Partikeltechnologie GmbH, Friedrich-Barnewitz-Str. 4, D-18119 Rostock, Germany.

[6] Division of Neuropathology, Department of Neurodegenerative Disease, UCL Institute of Neurology (ION), University College London (UCL), Queen Square, London WC1N 3BG, UK

[§] Authors contributed equally to this manuscript

***** Corresponding author (k.chester@ucl.ac.uk)

KEYWORDS: superparamagnetic iron oxide nanoparticles (SPIONs), ferucarbotran, reticuloendothelial system (RES), dextran, fucoidan, single-photon emission computed tomography (SPECT), positron emission tomography (PET).

ABSTRACT

The magnetic properties and safety of dextran-coated superparamagnetic iron oxide nanoparticles (SPIONs) have facilitated their clinical use as MRI contrast agents and stimulated research on applications for SPIONs in particle imaging and magnetic hyperthermia. The wider clinical potential of SPIONs, however, has been limited by their rapid removal from circulation *via* the reticuloendothelial system (RES). We explored the possibility of extending SPIONs circulatory time using fucoidan, a seaweed-derived food supplement, to inhibit RES uptake. The effects of fucoidan on SPION biodistribution were evaluated using ferucarbotran, which in its pharmaceutical formulation (Resovist®) targets the RES. Ferucarbotran was radiolabeled at the iron oxide core with technetium-99m (^{99m}Tc; $t_{1/2}$ = 6 hours) or zirconium-89 (^{89}Zr; $t_{1/2}$ = 3.3 days). Results obtained with ^{99m}Tc-ferucarbotran demonstrated that administration of fucoidan led to a 4-fold increase in the circulatory half-life ($t_{1/2}$ slow) from 37.4 to 150 minutes (n = 4; P < 0.0001). To investigate whether a longer circulatory half-life could lead to concomitant increased tumor uptake, the effects of fucoidan were tested with ^{89}Zr-ferucarbotran in mice bearing syngeneic subcutaneous (GL261) tumors. In this model, the longer circulatory half-life achieved with fucoidan was associated with a doubling in tumor SPION uptake (n = 5; P < 0.001). Fucoidan was also effective in significantly increasing the circulatory half-life of perimag®-COOH, a commercially available SPION with a larger hydrodynamic size (130 nm) than ferucarbotran (65 nm). These findings indicate successful diversion of SPIONs away from the hepatic RES and show realistic potential for future clinical applications.

Table of content graphic:

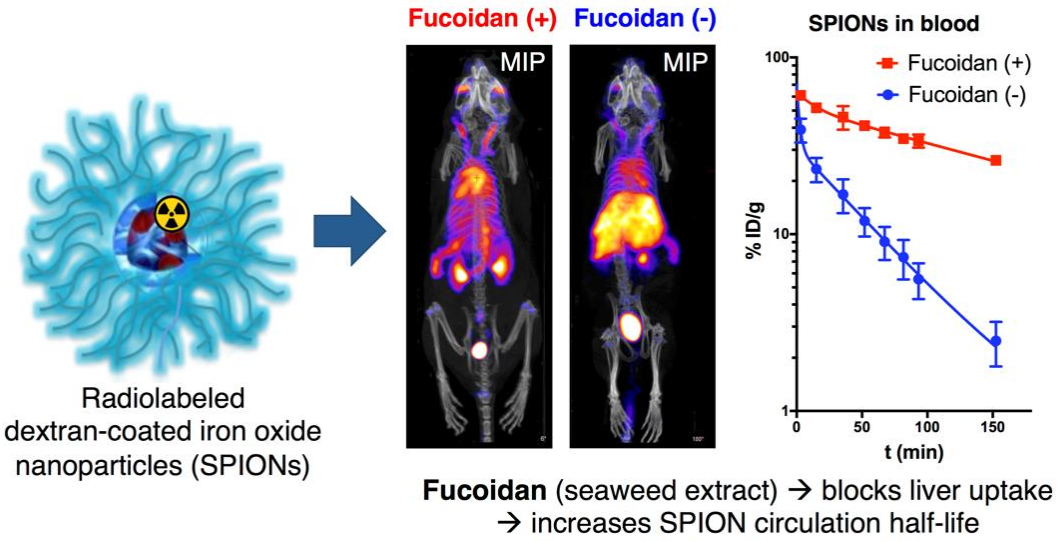

Dextran-coated superparamagnetic iron oxide nanoparticles (SPIONs) have many applications in biomedical research and a proven safety track record in clinical practice as contrast agents for magnetic resonance imaging (MRI) and as treatments for anemia.[1-4] Moreover, recent advances in magnetic hyperthermia therapy[5] and imaging techniques such as magnetic particle imaging (MPI)[6] and photoacoustic imaging[7] have resulted in an increased interest for SPION-based contrast agents. However, SPIONs show preferential uptake by *in situ* macrophages within the reticuloendothelial system (RES) of the liver and spleen. Therefore, use of SPIONs in the clinic to date has mainly been to detect malignant lesions within these tissues[8] or to image macrophage density in diseases such as atherosclerosis[8-11] and type 1 diabetes.[12]

The sequestration of SPIONs by the RES leads to very short circulation time and limits the wider imaging and therapeutic potential of SPIONs for non-RES targeted applications, such as tumor targeting through enhanced permeability and retention (EPR).[13] Various methods to increase the half-life of SPIONs have been explored, many utilizing coatings (such as high density polyethylene glycol (PEG) polymers), [14-17] designed to sterically prevent hydrophobic and electrostatic interactions with components of the blood.[14-18] The brush-like structures of the coat help to generate repulsive steric forces,[19] reduce the formation of a protein corona[20] and thus protect nanoparticles from recognition by macrophages.[21] Newer SPION modification technologies include bio-nano hybrid systems with biomimetic coatings, coating with 'self' peptides, or encapsulation within cell membranes.[22-28]

An alternative strategy to prolong SPIONs circulatory time is to pre-treat with agents that inhibit the innate immune system components responsible for the rapid clearance of nanoparticles, thereby imposing a temporary block on circulatory removal and potentially allowing greater access of SPIONs to other tissues. This 'blocking approach' has the advantage that there is no requirement for complex chemical modification of SPIONs and it can be readily applicable to SPIONs already approved for clinical use. A number of agents have been

investigated as potential blockers to facilitate SPIONs accessibility, *e.g.* clodronate liposomes to deplete macrophages, gadolinium chloride ($GdCl_3$) to inhibit Kupffer cell phagocytosis, complement inhibitors and the use of decoy nanoparticles to saturate macrophages prior to the injection of the therapeutic nanoparticles.[29] Whilst there is some evidence of promise, none have yet been taken forward to the clinic and potential toxicity is a concern. For instance, dextran sulfate 500 (DSO4 500) can be used to block macrophage uptake of ferucarbotran, the SPION component of Resovist®,[30] a clinical T2 MRI contrast agent designed to target the RES in order to detect focal liver cancerous lesions.[31] However, DSO4 500 is not suitable for clinical development due to its toxic side effects (*e.g.* reversible thrombocytopenia and alopecia).[32]

In the search for a clinically translatable alternative we turned our attention to fucoidans, a class of naturally occurring sulfated polysaccharides which are known ligands of the scavenger receptor class A (SR A).[33] SR A are responsible for macrophage uptake of dextran-coated SPIONs.[34-38] Fucoidans are composed mainly of fucose and sulfate ester groups and can be extracted from different species of brown seaweed (*e.g. Fucus vesiculosus, Undaria pinnatifida* and *Macrocystis pyrifera*) and marine invertebrates (*e.g.* sea urchins and sea cucumbers).[39,40] Seaweed is eaten in many cultures and seaweed extracts are readily available in many over the counter food supplements.[41] The safety profile of fucoidans makes them promising agents for clinical development and in recent years they have been subjected to intense research due to their versatile biological applications.[39,40, 42] Fucoidans are reported to possess antioxidant, antiviral, anticoagulant and anti-inflammatory properties, and to modulate blood lipid

levels.[39,40] Fucoidan has also been studied as an anticancer agent[43] and has been investigated in osteoarthritis, stem cell modulation, kidney disease and liver disease.[41]

In this study, we use radiolabeled SPIONs and *in vivo* preclinical nuclear imaging to investigate the biodistribution of dextran-coated SPIONs. We apply these methods to evaluate the potential of fucoidans to increase the circulatory presence of SPIONs and enhance tumor uptake.

RESULTS AND DISCUSSION

In vitro internalization and inhibition of ferucarbotran uptake by macrophages

The uptake of ferucarbotran was first evaluated *in vitro* using the murine monocyte/macrophage cell line RAW 264.7[44] that has been extensively employed in the study of the interactions of nanoparticles, specifically SPIONs, with macrophages.[35-37, 45] Ferucarbotran uptake by the cells was measured quantitatively by the ferrozine iron assay[46] and visualized using Prussian blue (Perls') staining.[47-51] Internalization of electron-dense SPIONs by cells was confirmed by transmission electron microscopy (TEM). The results, shown in Figure 1A, revealed that macrophage iron uptake increased in a dose dependent manner in proportion to the concentration of ferucarbotran incubated with the cells. This is consistent with the endocytosis of SPIONs by macrophages observed by others[36, 52] and thought to be mainly mediated *via* SR A[34-38] and clathrin-mediated endocytosis.[35,36] Studies investigating the role of other carbohydrate recognition pathways in SPION uptake indicate that, whilst mannose receptors (CD206) and SIGNR1 can mediate the uptake of bacterial polysaccharides such as dextrans, these receptors do not appear to be involved in the uptake of dextran coated SPIONs.[37]

Perls' staining is a long-established method to stain SPIONs in cells and tissues giving dense blue aggregates. Thus, the presence of blue aggregates within RAW 264.7 cells incubated with

ferucarbotran (Figure 1B) was taken to demonstrate the presence of SPIONs. TEM was used to show the internalization of ferucarbotran, which appears within the cells as aggregates rather than as single particles (Figure 1C). All intracellular nanoparticles detected were in cytoplasmic vesicles and none were visualized within the nucleus. Low magnification TEM images of macrophages showed invagination of the cell membrane (Figure 1D), indicating nanoparticle aggregates in the process of being endocytosed; non-internalized nanoparticles were visualized on the cell surface membrane. To test if the electron dense aggregates were SPIONs, energy dispersive X-ray (EDAX) microanalysis of unstained TEM slides was performed (Figure 1E-F). The presence of elemental iron indicated that the aggregates were indeed SPIONs, as opposed to other electron dense structures found within cells.

Fucoidans from 3 different species of seaweed: *Fucus vesiculosus* (FVF), *Macrocystis pyrifera* (MPF) and *Undaria pinnatifida* (UPF) were evaluated, in comparison with DSO4 500, for ability to reduce uptake of ferucarbotran by RAW 264.7 macrophages. Cells were pretreated with the fucoidans or DSO4 500 at concentrations of 30 and 60 μg/mL, followed by incubation with ferucarbotran at 0.1, 0.5 and 1 mgFe/mL. Results (Figure 1G), demonstrated that pre-treatment with fucoidans led to a significant reduction in the uptake of ferucarbotran at all

tested conditions. These results support published literature on the *in vitro* blocking effect of both DSO4 500[53] and fucoidan[54] on nanoparticle uptake by macrophages.

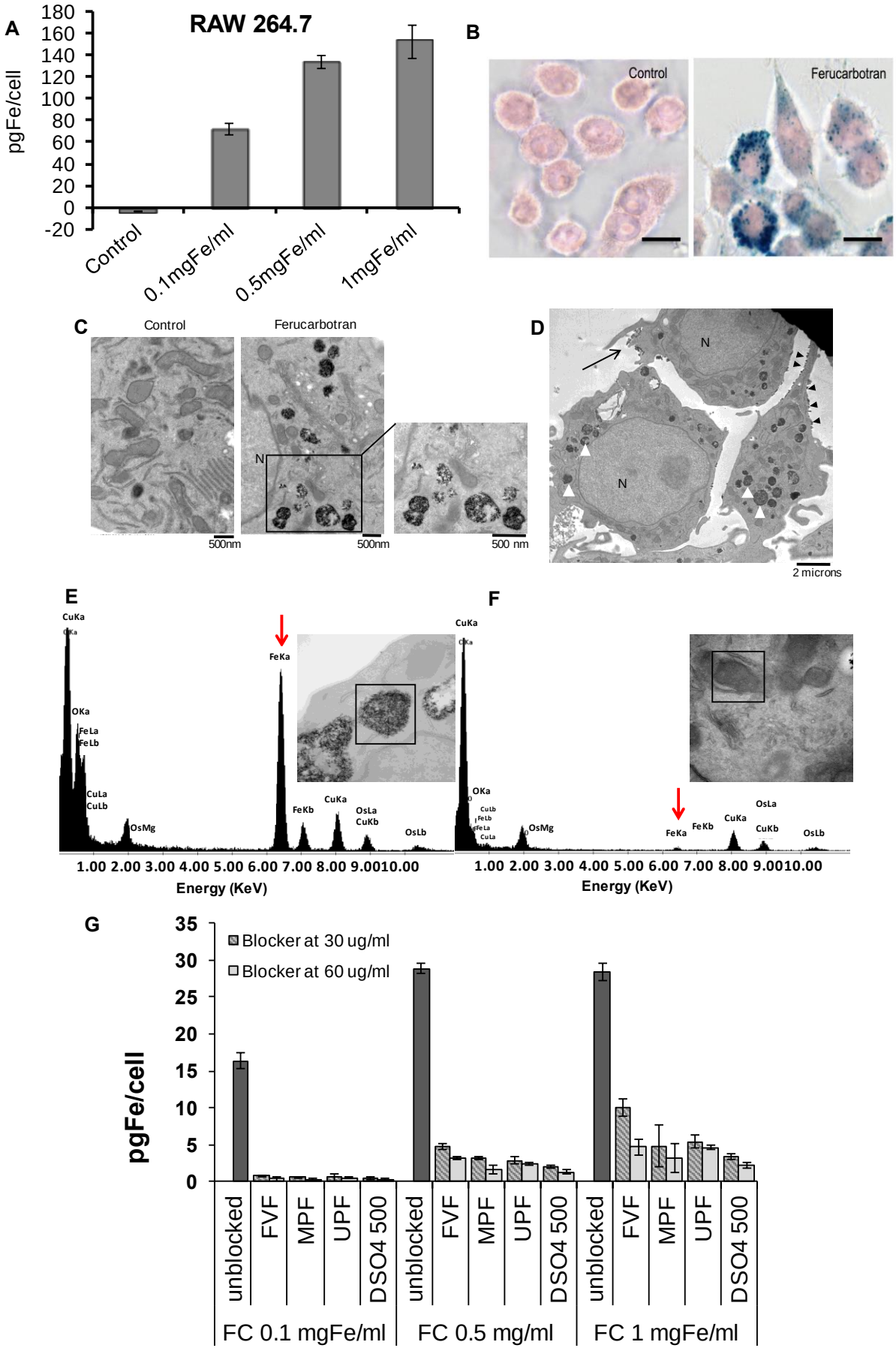
A
RAW 264.7
pgFe/cell
180
160
140
120
100
80
60
40
20
0
-20
Control
0.1mgFe/ml
0.5mgFe/ml
1mgFe/ml
B
Control
Ferucarbotran
C
Control
Ferucarbotran
N
500nm
500nm
500 nm
D
N
N
2 microns
E
CuKa
OKa
FeLa
FeLb
CuLa
CuLb
OsMg
FeKa
FeKb
CuKa
OsLa
CuKb
OsLb
1.00 2.00 3.00 4.00 5.00 6.00 7.00 8.00 9.00 10.00
Energy (KeV)
F
CuKa
OKa
OsMg
FeKa
FeKb
CuKa
OsLa
CuKb
OsLb
1.00 2.00 3.00 4.00 5.00 6.00 7.00 8.00 9.00 10.00
Energy (KeV)
G
Blocker at 30 ug/ml
Blocker at 60 ug/ml
pgFe/cell
35
30
25
20
15
10
5
0
unblocked
FVF
MPF
UPF
DSO4 500
FC 0.1 mgFe/ml
FC 0.5 mg/ml
FC 1 mgFe/ml

Figure 1. Internalization of ferucarbotran by macrophages. (**A)** Ferrozine assay was used to measure the uptake of ferucarbotran by macrophages. Bars represent the average of 3 replicates; error bars are for standard deviation. (**B)** Prussian blue staining showed the presence of ferucarbotran as blue aggregates inside the cells compared to none visible in the untreated control. Scale bar = 20 μm (**C)** TEM micrographs showing electron dense cytoplasmic vesicles containing the SPIONs with none detected in the nucleus (N) or the untreated control. (**D)** Low magnification TEM image (6000x) showed some nanoparticles being endocytosed by macrophages (black arrow) while others appeared either on the surface of the cells attached to the cell membrane (black arrow heads) or inside the cells (white arrow heads). (**E-F)** EDAX microanalysis detected iron peaks (red arrow, E) in the vesicles containing the rod-shaped aggregates compared to no iron peak (red arrow, F) in other uniformly shaped electron dense vesicles inside the cells. **(G)** *In vitro* blocking effect of the three different fucoidans on the uptake of ferucarbotran by RAW 264.7 macrophages, compared to DSO4 500.

In vivo effect of fucoidan on the circulation time and biodistribution of ferucarbotran

Preliminary *in vivo* experiments were conducted using NIR-labeled ferucarbotran, a method previously established as suitable to measure blood concentrations of this nanoparticle.[30] These experiments confirmed that all three fucoidans were capable of significantly increasing the blood levels of ferucarbotran, demonstrable at one hour following particle injection. FVF was at least as effective as the other fucoidans (Supplementary Figure S1) and was taken forward because it was the best characterized and least poly-dispersed fucoidan (see supplementary data, tables S2-S4). An *in vivo* dose of 15 mg/kg was chosen based upon existing safety and tolerability data (Supplementary data, Biological safety and dose justification of *Fucus vesiculosus* (FVF)). To quantitate the effects of FVF on biodistribution, ferucarbotran was radiolabeled with the gamma-emitting radioisotope technetium-99m (^{99m}Tc) to track its organ uptake using SPECT/CT and by *ex vivo* gamma counting. The radiolabeling method exploits the high affinity of a bifunctional bisphosphonate chelator (dipicolylamine-alendronate; DPA-Ale) for the metal oxide core of ferucarbotran (Figure 2) and is an established technique previously shown to be capable of maintaining the original physicochemical properties of iron oxide nanoparticles (Supplementary Table S5).[55,56] This method has been successfully used in several studies to evaluate the biodistribution of SPIONs *in vivo* and shows negligible leakage of ^{99m}Tc-DPA-ale *in vivo* (Supplementary Figure S2).[55-59] Labeling SPIONs using

radionuclides has significant advantages over other imaging strategies (*e.g.* MRI or optical imaging) as it allows accurate quantitative information of their biodistribution at the whole-body level.

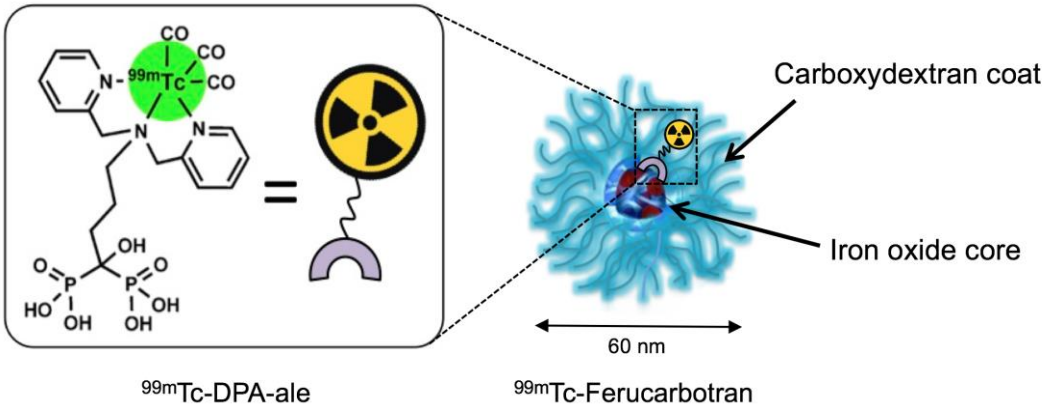

Figure 2. Schematic representation of ferucarbotran radiolabeling with ^{99m}Tc using a radiolabeled bifunctional bisphosphonate (^{99m}Tc-DPA-ale). The linker (DPA-ale; inset) is radiolabeled with ^{99m}Tc at the dipicolylamine (DPA) group while the bisphosphonate group effectively binds to the iron oxide core of the SPION.

Balb/c mice were injected *i.v.* with ^{99m}Tc–ferucarbotran (15-30 MBq, 34.8 μg Fe), immediately preceded either by an *i.v.* injection of FVF (FVF (+); n = 5) or PBS (FVF (-); n = 5). Selected animals from both groups were scanned using SPECT/CT for 80 minutes following injection (4 × 20 minutes scans) before being sacrificed and the organs harvested. To investigate circulation time, blood samples were obtained at set time points post ferucarbotran injection; either pretreated with FVF (n = 4) or PBS (n = 4).

The results showed a significant change in the pharmacokinetic behavior of ferucarbotran in the FVF-treated mice when compared to the controls (Figure 3A). The circulation half-life ($t_{1/2}$) and the area under the curve (AUC), calculated using a two-compartment pharmacokinetic model from the blood sampling results, revealed that FVF increased the $t_{1/2}$ (slow) 4-fold, from 37.4 to 150 minutes (n = 4; P < 0.0001). In addition, the AUC, representative of the total

exposure of the animals to systemically circulating SPIONs, increased 3.5-fold, from 1615 ± 93 %ID · min/g to 5699 ± 138 %ID · min/g (n = 4; P < 0.0001).

SPECT/CT imaging (Figure 3B) showed that in the control group (FVF (-)), ^{99m}Tc-ferucarbotran was clearly visualized in the liver 20 minutes post injection with minor presence in the bloodstream. In contrast, in FVF treated mice (FVF (+)), ^{99m}Tc–ferucarbotran was mainly detected within the blood pool. At 80 minutes post injection, ^{99m}Tc–ferucarbotran was visualized mainly within the liver for FVF (-) mice, whereas in FVF (+) mice, a blood pool presence was still observed, with only minor uptake in the liver. These findings support the hypothesis that FVF is able to block the uptake of ^{99m}Tc–ferucarbotran by liver macrophages, and significantly prolong the circulatory time of the SPION. The signal observed in the bladder of FVF (+) mice is likely to correspond to a small fraction of excreted metabolized radionuclide, as previously reported for long-circulating PEGylated iron oxide nanoparticles radiolabeled using this method.[55]

Following imaging studies, *ex vivo* ^{99m}Tc–ferucarbotran organ counts were performed and expressed in percentage of injected dose per gram of tissue (%ID/g). Consistent with the findings on SPECT/CT, the most striking differences were the decreased %ID/g in liver with concomitant increases in both blood and spleen (Figure 3C-D). Furthermore, tissue to blood ratios demonstrated significant differences in the uptake within the liver, with a liver to blood ratio of 8.3 ± 2.8 compared to only 0.5 ± 0.1 in the FVF (+) counterpart (n = 5; P < 0.01). However, there was no significant difference in tissue to blood ratios for spleen, indicating that the increased %ID/g value for this organ was due to the higher blood levels. All other tissues showed similar tissue to blood ratios in the FVF (+) *vs.* FVF (-) groups. After radioactive decay, sections of the excised livers were stained using Prussian blue to determine whether the reduced liver uptake of SPIONs in the FVF treated mice could be visualized histologically. The resulting images indicated that staining appeared to be lower and less intense in the livers of

mice pretreated with FVF (Supplementary Figure S3A). Digital image analysis, performed to obtain a less subjective measurement, supported the observation that Perls' stain uptake in FVF treated mice (n = 2) was reduced overall and less intense than in the control mice (n = 2) (Supplementary Figure S3B). These results further support the hypothesis that FVF blocks the uptake of dextran-coated SPIONs, such as ferucarbotran, within the liver, although the mechanism by which SPION uptake is inhibited remains unclear. As ligands of SR A,[33] fucoidans could simply compete with and inhibit SR A uptake of dextran-coated SPIONs by macrophages. However, other receptors and immune recognition pathways may also be involved, leading to complex uptake mechanisms. Furthermore, SPIONs are known to develop a 'corona' of proteins when exposed to biological milieu, which can influence both their biocompatibility and biological fate.[60,61] There is evidence that the presence of complement proteins within this corona can affect the interactions of SPIONs with cells of the immune system,[62] directly influencing the interactions of the particles with immune cells, including internalization *via* scavenger receptors.[63,64]

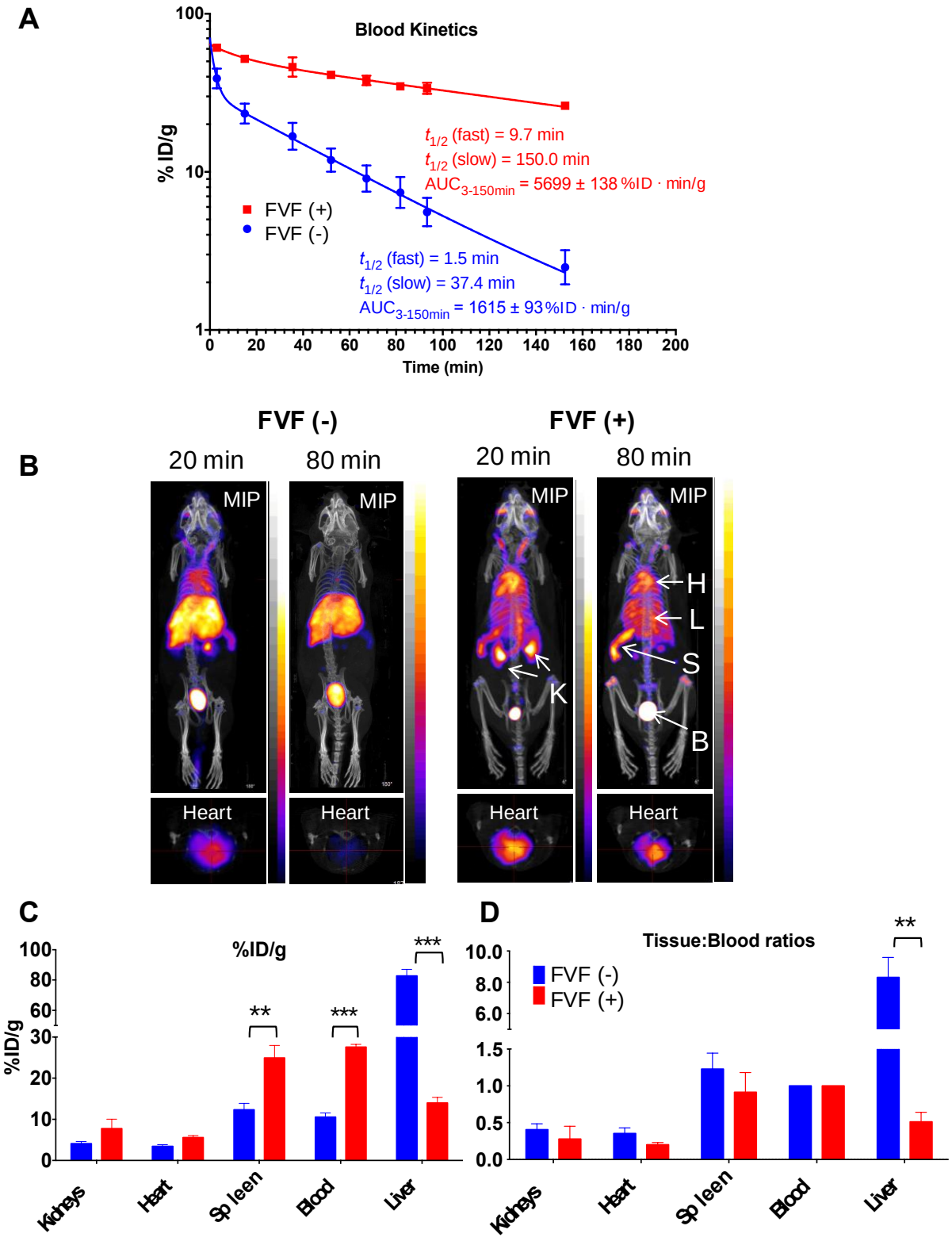
A
Blood Kinetics
% ID/g
Time (min)
FVF (+)
FVF (-)
t1/2 (fast) = 9.7 min
t1/2 (slow) = 150.0 min
AUC3-150min = 5699 ± 138 %ID · min/g
t1/2 (fast) = 1.5 min
t1/2 (slow) = 37.4 min
AUC3-150min = 1615 ± 93 %ID · min/g
B
FVF (-)
FVF (+)
20 min
80 min
MIP
Heart
H
L
S
K
B
C
%ID/g
Kidneys
Heart
Spleen
Blood
Liver
D
Tissue:Blood ratios

Figure 3. Biodistribution of ^{99m}Tc-ferucarbotran in Balb/c mice. (A) Blood time-activity curve of ^{99m}Tc–ferucarbotran in the presence (+) and absence (-) of FVF (n = 4 per group). The data was fitted to a two-compartment pharmacokinetic model that allowed the calculation of the circulation half-life ($t_{1/2}$) and area under the curve (AUC) values for each group and showing a significant increase in circulation time in the FVF treated group. **(B)** Maximum intensity projection (MIP) images with transverse slices centered at the heart (bottom). H: heart; L: liver; S: Spleen; B: bladder and K: kidneys. **(C-D):** Biodistribution of ^{99m}Tc-ferucarbotran in post-mortem harvested organs 80 minutes following SPION injection (n = 5). *** $P < 0.0001$ and ** $P < 0.01$ compared to FVF (-) as measured with unpaired two-tailed t-test. Bars represent means and error bars are for the standard error of means (SEM). Full organ data can be found in Supplementary Tables S8 and S9.

Evaluating the effect of FVF blocking on the accumulation of SPIONs in tumors

In order to track ferucarbotran for longer time periods, the iron-oxide cores of the SPIONs were directly radiolabeled with the positron-emitter zirconium-89 (^{89}Zr; $t_{1/2}$ = 3.3 days), using a recently described method shown schematically in Figure 4.[65] This method caused an increase in the hydrodynamic diameter of ferucarbotran following labeling (z-average: 53.6 ± 0.1 to 127 ± 14 nm) as determined by dynamic light scattering (DLS) (Supplementary Table S6). Despite this increase in hydrodynamic size, ^{89}Zr-ferucarbotran remained in dispersion with no evidence of precipitation. This increase in size could result in more rapid circulatory clearance as larger SPIONs are known to possess shorter half-lives[66] and we predicted it could be more challenging to maintain ^{89}Zr-ferucarbotran in circulation, compared with ^{99m}Tc-ferucarbotran. To evaluate whether FVF could meet this challenge and also lead to a concomitant increase in accumulation of SPIONs within tumors, the subcutaneous GL261 syngeneic C57BL/6 mouse model was utilized.[67] GL261 has been extensively used to assess the efficacy of anti-cancer therapies including immunotherapies for the treatment of gliomas.[68,69] Another advantage of utilizing C57BL/6 mice was to test whether FVF is also active in strains of mice other than Balb/c.

^{89}Zr-ferucarbotran was injected *i.v.* into tumor bearing mice either without FVF (FVF (-); n = 5), immediately preceded by FVF (FVF (+) (pre-injection); n = 5) or with FVF included in the

SPION formulation (FVF (+) (co-injection); n = 5). Blood samples were taken at set time intervals, PET/CT imaging was performed at 30 minutes and 24 hours post injection and *ex vivo* organ counting performed at 24 hours.

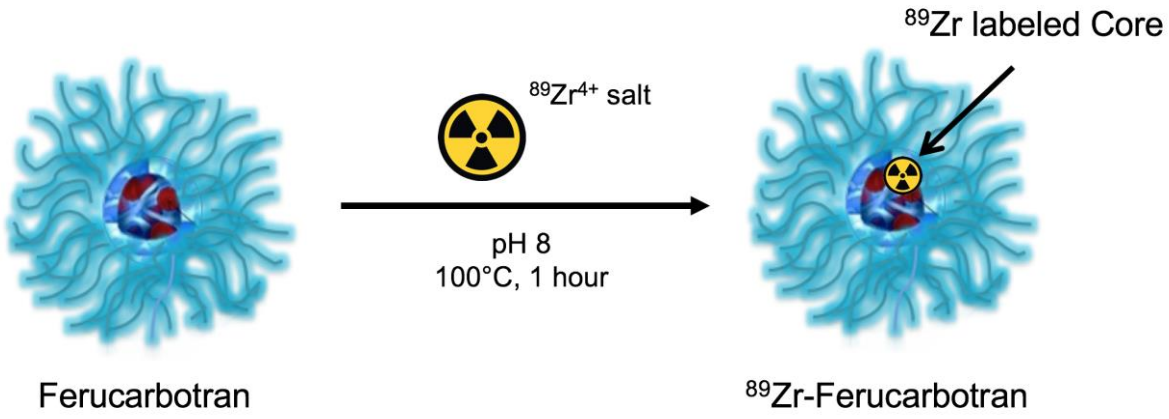

Figure 4. Schematic representation of the direct radiolabeling of ferucarbotran with ^{89}Zr.

Results showed that, consistent with the observed increase in hydrodynamic size, the circulatory clearance of ^{89}Zr-ferucarbotran occurred faster than that previously observed for ^{99m}Tc-ferucarbotran (Figure 5A). Nonetheless, FVF was able to increase ^{89}Zr-ferucarbotran circulation half-life, with a 2.3-fold increase in $t_{1/2}$ (slow), from 16.8 to 39.7 minutes (n = 3; P = 0.0006) and a 6-fold increase in AUC (from 176 ± 14 %ID · min/g to 1079 ± 89 %ID · min/g; n = 3; P = 0.0006). Results showed there was no significant difference between the FVF (+) (pre-injection) and FVF (+) (co-injection) groups (Figure 5A) (Note: FVF (+) pharmacokinetic data refers to the pre-injection method only, as the co-injection method data could not be fitted to the two-compartment pharmacokinetic model).

PET images were obtained at 30 minutes post-injection (Figure 5B), showing observable differences between FVF (+) and FVF (-) groups in liver uptake, with no PET signal detected in the blood pool in any of the groups. A lower ^{89}Zr-ferucarbotran signal was observed by PET/CT in the liver of FVF (+) mice with higher observed signal in the spleen at both 30

minutes and 24 hours following injection. Within tumors, a higher signal was observed in the tumors of FVF (+) mice at both time points. *Ex vivo* organ counting (%ID/g) at 24 hours showed patterns of uptake consistent with PET/CT observations, with significantly higher %ID/g in the blood (P = 0.0432), spleen (P = 0.0017) and heart (P = 0.0082) of FVF treated mice (pre-injection) (Figure 5C-D). Concomitant with the increased circulatory presence, administration of FVF also led to a 2-fold increase in the tumor accumulation of SPIONs (P < 0.001). In summary, these results indicate that blocking SPION uptake into RES macrophages leads to increased circulatory presence and greater tumor uptake.

Within the tumor, fucoidan could react with tumor associated macrophages (TAMs) giving rise to a number of effects that warrant further study. TAMs are phenotypically plastic and their roles in the tumor microenvironment are complex and contrasting. They can promote cancer-related inflammation and tumor progression by a number of mechanisms and they can also exhibit antitumor effects.[70] SPIONs have been shown to influence macrophage polarization[71,72] and may consequently inhibit tumor growth.[71] In this instance, the potentially undesirable effects of inhibiting SPION uptake by TAMs should be considered. Independent of its SPION-blocking function, fucoidan could affect tumor growth *via* direct interaction with SRs on the cell surface of TAMs. SR has been reported to contribute to immunosuppression[43] and promote tumor progression[73] and the interactions between fucoidan and SR within the tumor microenvironment have been implicated as contributory to fucoidan's purported anti-cancer effects.[43] Other studies suggest that fucoidan binding to SR leads to dendritic cell activation, enhancing the immune response. Furthermore, fucoidan has been shown to possess immune-stimulating effects on both DCs[74-77] and natural killer (NK) cells[78,79] and therefore could also enhance anticancer immunity by activating immune cells and stimulating production of immunostimulatory cytokines.[43]

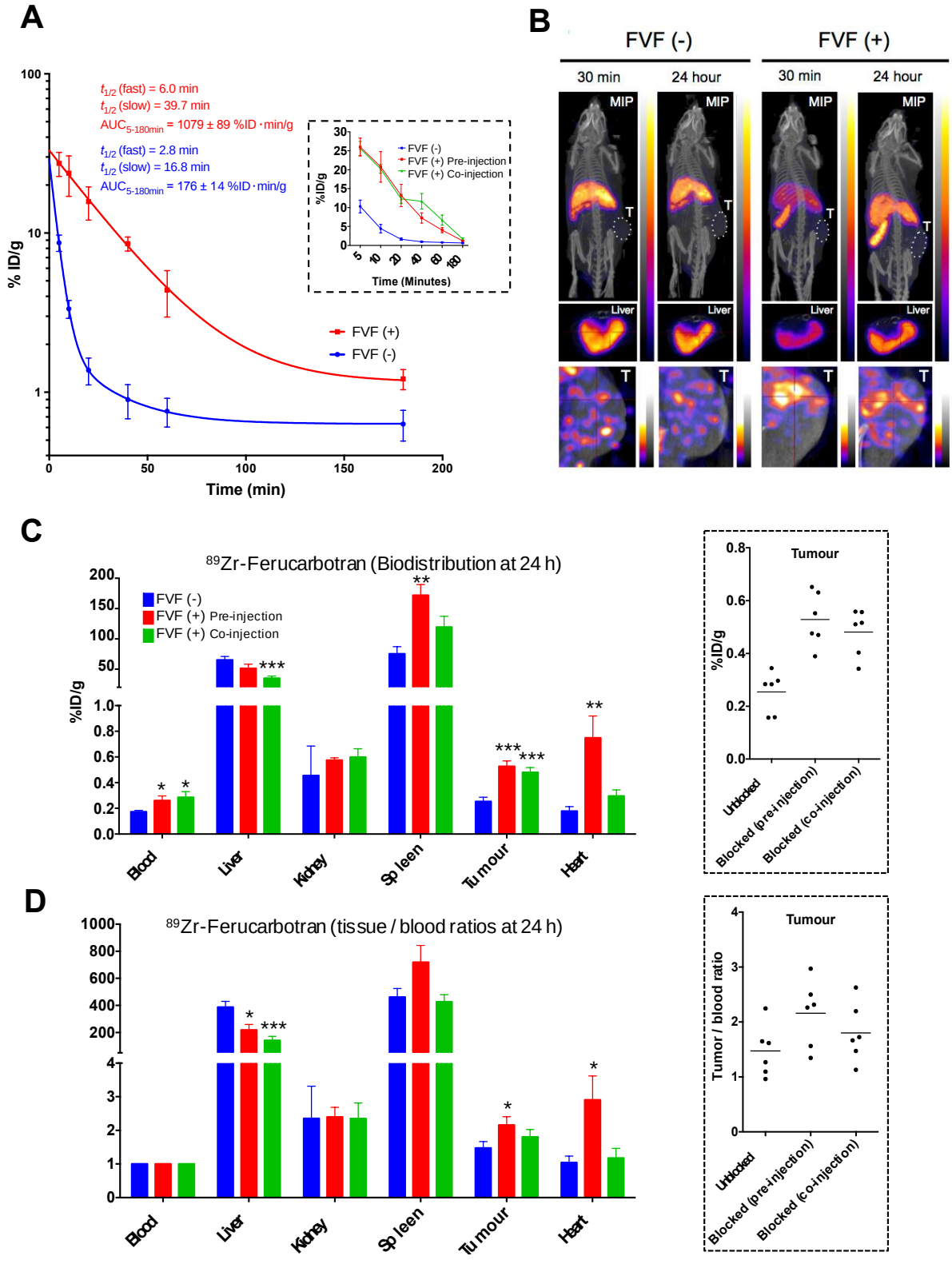
A
$t_{1/2}$ (fast) = 6.0 min
$t_{1/2}$ (slow) = 39.7 min
$AUC_{5\text{-}180min}$ = 1079 ± 89 %ID·min/g
$t_{1/2}$ (fast) = 2.8 min
$t_{1/2}$ (slow) = 16.8 min
$AUC_{5\text{-}180min}$ = 176 ± 14 %ID·min/g
% ID/g
Time (min)
FVF (+)
FVF (-)
%ID/g
Time (Minutes)
FVF (-)
FVF (+) Pre-injection
FVF (+) Co-injection
B
FVF (-)
FVF (+)
30 min
24 hour
MIP
Liver
T
C
89Zr-Ferucarbotran (Biodistribution at 24 h)
%ID/g
Blood
Liver
Kidney
Spleen
Tumour
Heart
Tumour
Untdocked
Blocked (pre-injection)
Blocked (co-injection)
D
89Zr-Ferucarbotran (tissue / blood ratios at 24 h)
Tumor / blood ratio

Figure 5. Blood clearance and systemic biodistribution of ^{89}Zr-Ferucarbotran in tumor bearing C57BL/6 mice. (**A**) Blood time-activity curve in the presence and absence of FVF (Inset: comparison of the pre- and co-injection methods showing no difference in the effect of FVF. Note linear scale in y-axis). (**B**) Maximum intensity projection images (MIP) with transverse slices centered at the liver and tumor taken at 30 minutes and 24 h post injection of ^{89}Zr-ferucarbotran. Since no significant difference was observed between the pre-injection and the co-injection FVF-treated mice; 'FVF (+)' refers to the pre-injection group in Figure 5B. (**C-D**): Biodistribution of ^{89}Zr-ferucarbotran in select post-mortem harvested organs at 24 h post injection. Inset shows the tumor uptake. *** $P \leq 0.001$, ** $P < 0.01$ and * $P < 0.05$ compared to FVF (-) as measured using an unpaired two-tailed t-test. Bars represent mean values and error bars are for the standard error of the mean (SEM). Full organ data can be seen in Supplementary Tables S10 and S11.

Testing the effects of fucoidan on the uptake of perimag® SPIONs *in vitro*

To determine whether the blocking effects of fucoidan were applicable to other SPIONs, FVF was tested on perimag® (Table 1), a family of SPIONs with favorable properties for magnetic resonance and magnetic particle imaging, stem cell tracking, and hyperthermia therapy.[80-81] There are a number of differences between perimag® SPIONs and ferucarbotran; ferucarbotran is coated with carboxydextran and has a hydrodynamic diameter of approximately 65 nm, whilst perimag®-COOH is significantly larger (130 nm) and has a plain dextran coating (perimag®-plain) subsequently functionalized with carboxylic acid groups. Thus, perimag® can be controlled in terms of the quantity of surface carboxylic acid groups, providing a versatile basis for SPION development. Perimag®-plain can also be functionalized with positively charged amine groups (perimag®-NH_2).

Table 1. SPIONs investigated in this study.

Reagent Name	Coat	Supplier	Size from manufacturer	Surface Charge (Zeta-potential) *
Ferucarbotran	Carboxydextran	Meito-Sangyo, Japan	65 nm	-20.0 ± 11.0 mV
Perimag®-plain	Dextran	Micromod GmbH, Germany	130 nm	-1.47 ± 5.01 mV
Perimag®-COOH	Dextran functionalized with carboxylic acid groups		130 nm	-9.94 ± 3.38 mV
Perimag®-NH_2	Dextran functionalized with amine groups		130 nm	13.00 ± 3.72 mV

** Measured in 5 mM NaCl on a Zetasizer Nano ZS90 (Malvern, Worcestershire, UK)*

First, the interaction of perimag® SPIONs with RAW 264.7 macrophages was investigated and the effects of fucoidan on this interaction evaluated. The results (Figure 6) revealed that all perimag® SPIONs had lower macrophage uptake than ferucarbotran, with only perimag®-COOH showing strong uptake. Cellular uptake of the near-neutral perimag®-plain and the positively charged perimag®-NH_2 was low, irrespective of whether fucoidan or DSO4 500 were present. These *in vitro* findings are consistent with the predisposition of macrophages to take up negatively charged particles.[82] The relatively lower macrophage uptake of perimag®-COOH compared to ferucarbotran could be attributable to the differences in their charge or hydrodynamic diameters as previously observed with other particles.[83]

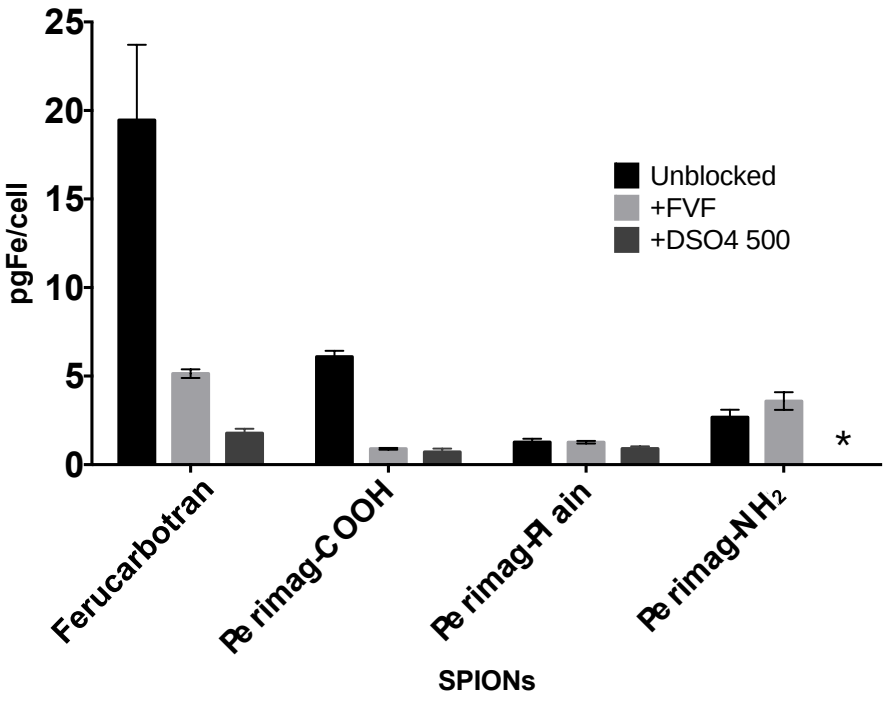

Figure 6. Testing the effect of fucoidan (FVF) and dextran sulfate (DSO4 500) on the uptake of different SPIONs by RAW 264.7 macrophages. Equimolar concentrations (0.17 μM) of FVF and DSO4 500 were used. *DSO4 500 led to the precipitation of perimag®-NH_2. Bars represent the mean value and error bars are for standard deviation.

Treatment with FVF or DSO4 500 significantly reduced macrophage uptake of perimag®-COOH providing justification to test whether FVF would be an effective RES blocker of perimag®-COOH *in vivo.* As well as being predisposed to uptake by macrophages, negatively charged SPIONs show promise for clinical development because they possess superior biocompatibility compared to their positively charged and neutral counterparts.[84]

Testing the effect of FVF on the biodistribution of perimag®-COOH

Perimag®-COOH was radiolabeled with ^{89}Zr as described for ferucarbotran (Figure 4). The perimag® SPIONs showed superior labelling stability as, in contrast to ^{89}Zr-ferucarbotran, ^{89}Zr-perimag®-COOH did not show any significant change in size when analyzed by DLS (Supplementary Table S7). ^{89}Zr-perimag®-COOH was injected *i.v.* into C57BL/6 mice either alone (FVF (-), with a preceding injection of fucoidan (FVF (+) pre-injection) or in

combination with fucoidan (FVF (+) co-injection). As described previously, blood samples were taken at pre-determined time points, mice were imaged by PET/CT at 80 minutes and 24 hours and organ counts were conducted at 80 minutes and 24 hours following injection.

The results showed a clear change in the pharmacokinetic behavior of ^{89}Zr-perimag®-COOH in the FVF (+) mice compared to FVF (-) control (Figure 7A). Similar to the results observed using ^{99m}Tc–ferucarbotran and ^{89}Zr–ferucarbotran, FVF caused an increase in the systemic circulation of ^{89}Zr-perimag®-COOH in FVF (+) mice, with a calculated AUC of 484 ± 44 %ID · min/g and 566 ± 76 %ID · min/g (n = 3; P = 0.18) for the FVF pre-injection and FVF co-injection groups, respectively, compared to 183 ± 14 for the FVF (-) control. Once again, this result demonstrated that there was no significant difference observed between the FVF pre-injection and the co-injection groups. Overall, the administration of FVF led to a 2.6-fold increase in the AUC of ^{89}Zr-perimag®-COOH and a 1.6-fold increase in the circulation half-life ($t_{1/2}$ slow) from 18.9 minutes (FVF (-)) to 30.7 minutes (FVF (+) pre-injection) (n = 3; P = 0.004). PET/CT images and the *ex-vivo* biodistribution data (Figure 7B-G) revealed that ^{89}Zr-perimag®-COOH cleared faster than ^{99m}Tc–ferucarbotran. For all groups, at 80 minutes, a very low %ID/g remained within the blood pool with the majority of the SPIONs observed within the liver and the spleen. This could be explained by the larger hydrodynamic diameter of ^{89}Zr-perimag®-COOH compared to ^{99m}Tc-ferucarbotran resulting in faster clearance by the RES. Nonetheless, PET imaging appeared to show a lower signal in the liver of mice treated with FVF compared to the FVF (-) controls. Tissue to blood ratios at 80 minutes showed a lower ratio in the liver for mice treated with FVF, although these differences were not found to be statistically significant. In summary, FVF successfully increased the circulatory half-life of perimag®-COOH confirming that this finding was not limited to ferucarbotran.

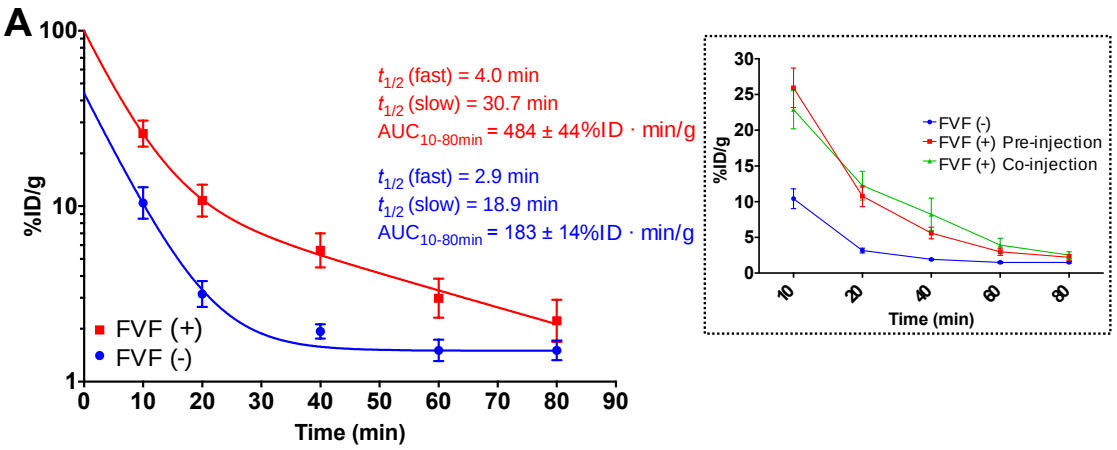
A
%ID/g
Time (min)
FVF (+)
FVF (-)
t1/2 (fast) = 4.0 min
t1/2 (slow) = 30.7 min
AUC10-80min = 484 ± 44%ID · min/g
t1/2 (fast) = 2.9 min
t1/2 (slow) = 18.9 min
AUC10-80min = 183 ± 14%ID · min/g
FVF (-)
FVF (+) Pre-injection
FVF (+) Co-injection

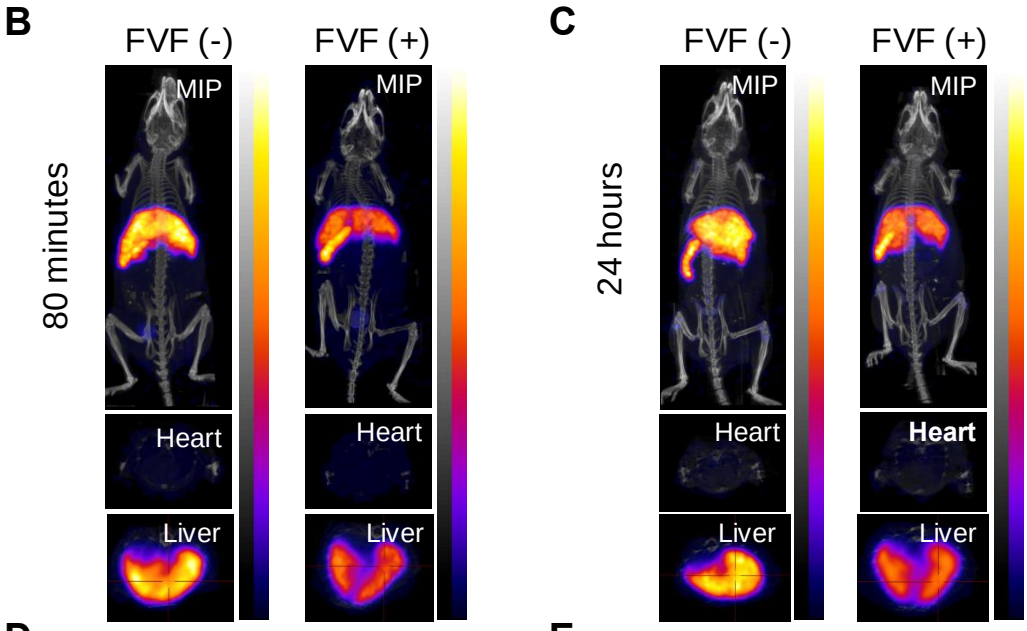
B
FVF (-)
FVF (+)
80 minutes
MIP
Heart
Liver
C
24 hours

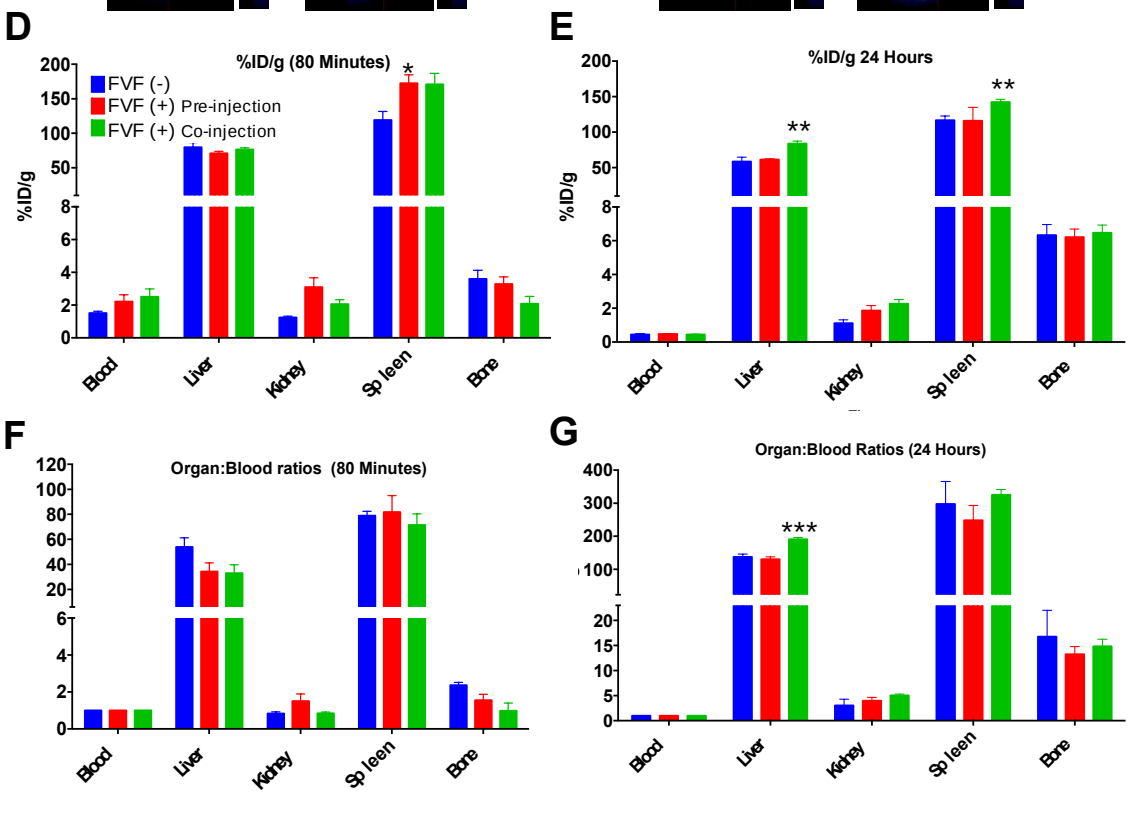
D
%ID/g (80 Minutes)
FVF (-)
FVF (+) Pre-injection
FVF (+) Co-injection
%ID/g
Blood
Liver
Kidney
Spleen
Bone
E
%ID/g 24 Hours
F
Organ:Blood ratios (80 Minutes)
G
Organ:Blood Ratios (24 Hours)

Figure 7. Biodistribution of ^{89}Zr-perimag®-COOH in C57BL/6 mice. (A) Blood time-activity curve in the presence and absence of FVF. The data was fitted to a two-compartmental pharmacokinetic model that allowed the calculation of the circulation half-lives ($t_{1/2}$) and areas under the curve (AUC) values for each group (Inset: comparison of the pre- and co-injection methods showing no difference in the effect of FVF. Note linear scale in y-axis) **(B, C)** Maximum intensity projection images (MIP) with transverse slice (bottom) centered at the heart and liver taken at 80 minutes (B) and 24 hours (C) post injection of ^{89}Zr-perimag®-COOH. FVF (+) refers to the pre-injection group**. (D-G):** Biodistribution of ^{89}Zr-perimag®-COOH in post-mortem harvested organs at 80 min (D) and 24 h (E). *** $P = 0.001$, ** $P = 0.01$ and * $P < 0.05$ compared to FVF (-) as measured with unpaired two-tailed t-test. Bars represent means and error bars are for the standard error of means (SEM). Full organ count data is available in Supplementary Tables S12, S13, S14 and S15.

CONCLUSIONS

Rapid circulatory clearance is considered one of the major limitations in the development of nanoparticles. We report a perspective to prolong the half-life of one class of nanoparticle, dextran-coated SPIONs, without the need to change their physicochemical characteristics.

In summary, we used two different radiolabeling strategies (^{99m}Tc and ^{89}Zr) to trace two types of SPIONs (ferucarbotran and perimag®-COOH) with high sensitivity *in vivo*. By employing fucoidan, a naturally occurring polysaccharide, we prolonged the circulation half-lives of SPIONs, increased their systemic presence (AUC) and doubled their accumulation in tumors. Fucoidan is readily available as a natural food supplement with no reported toxic side effects either *in vitro* or *in vivo*.[43]

There are ongoing discussions regarding the effectiveness of nanoparticle delivery, with concern that over the last decade the average delivery of systemically administered particles to tissues of interest has remained below 1% of the administered dose, despite the utility of both passive and active targeting.[85,86] Sequestration of particles by the RES is a major factor in this low delivery and by prolonging the circulation time, fucoidan could work synergistically with

passive and active targeting technologies, providing a generic means to improve the delivery of many different nanoparticles.

Removal of nanoparticles by the RES leads to a lack of efficacy because the particles are sequestered away from the intended sites of delivery and into the liver and spleen.[22, 87] Approaches for RES avoidance have long been sought and is most commonly tackled by modifying SPIONs coatings with hydrophilic polymer coatings (*e.g.* PEG, PVP, poloxamines and poloxamers) to prolong circulation times.[88] However, modifying the surface coatings in this way changes the physical properties of the nanomaterial and is therefore unsuitable when using clinical products with well-studied safety profiles. By overcoming the rapid RES clearance of SPIONs, the work presented in this paper could provide a step towards the clinical development of nanomedicines.

EXPERIMENTAL SECTION

Materials. Ferucarbotran was purchased from Meito Sangyo Co. LTD., Tokyo, Japan. Perimag® was obtained from Micromod Partikeltechnologie GmbH. All other materials were purchased from Sigma Aldrich (Dorset, UK) unless otherwise specified.

Cell uptake experiments. All *in vitro* experiments were repeated at least 3 times on 3 different days for reproducibility and representative data is shown in the results section. RAW 264.7 cells were seeded at 2 x 10^5 cells/well in 24-well plates (Corning®) and left to attach overnight. On the following day, the cells were treated with ferucarbotran at three different concentrations (0.1, 0.5, 1 mgFe/mL) for 4 hours at 37°C. Cells were then washed 3 times with cold PBS to remove excess unbound SPIONs. Next, the cells were lysed with 200 μL of 50 mM sodium hydroxide (NaOH) and the intracellular iron content was determined using the colorimetric ferrozine assay[46] and then compared to a standard curve of ferucarbotran samples of known

iron concentrations. For the ferrozine assay; 100 μL of each cell lysate was aliquoted into an Eppendorf tube then 100 μL of dH_2O (solvent of ferucarbotran) was added. 100 μL aliquots of serial dilutions of ferucarbotran at 0.15 - 20 μgFe/mL were prepared from the stock solution and then 100 μL of 50 mM NaOH was added to each tube. Next, to each tube of cell lysates and ferucarbotran, 100 μL of freshly prepared iron releasing solution (equal volumes of 1.4 M HCl and 4.5% (w/v) potassium permanganate ($KMnO_4$)) was added. The mixture was incubated for 2 hours at 60 °C in a water bath before being cooled down for 10 minutes followed by the addition of 30 μL of iron detection solution (6.5 mM neocuproine, 6.5 mM ferrozine, 1 M ascorbic acid and 2.5 M ammonium acetate in water). The tubes were then further incubated for 30 minutes to allow for maximum color development. 100 μL of each tube was then aliquoted into a 96-well plate (Corning®) and the absorbance was measured at 550 nm on Varioskan™ Flash Multimode reader (Thermo Scientific). The concentration of each sample was extrapolated from the standard curve and the amount of iron per cell (picograms iron per cell (pgFe/cell)) was calculated as follows:

$$pgFe/cell = \frac{\text{Concentration } (mgFe/ml)}{\text{number of cells / ml}} X\,10^6$$

Perl's Prussian blue staining. Cells were seeded and treated with 0.5 mgFe/mL of ferucarbotran for 4 hours as described above. Next, the cells were washed thoroughly with cold PBS and fixed using a solution of 2% formalin and 2.5% glutaraldehyde in PBS for 10 minutes at room temperature. The cells were then washed with PBS and stained with a freshly prepared Prussian blue staining solution (4 g potassium hexacyanoferrate (II) trihydrate dissolved in 20 mL dH_2O + 20 mL 2% HCl) for 10 minutes and counterstained with eosin, mounted with DPX

and imaged with 100x oil immersion lens using Carl Zeiss Axioskop MOT 2 microscope (Carl Zeiss, Germany).

Transmission Electron Microscopy (TEM) and Energy Dispersive X-ray microanalysis (EDAX). Cells were seeded at 2 x 10^5 cells/well in 6-well plates (Corning®) and allowed to attach overnight. Next day the cells were treated with 0.5 mgFe/mL ferucarbotran for 4 hours before being washed 3 times with cold PBS. Then the cells were fixed in 1.5% glutaraldehyde/1% paraformaldehyde/PBS pH 7.4, for a minimum of 2 hours, and stored at 4°C until processing for TEM. Fixed cells were centrifuged to form a pellet in 0.5 mL Eppendorf. The cells were then washed with two changes of phosphate buffer (Oxoid) and post-fixed with osmium tetroxide solution (1% osmium tetroxide (Analar BDH) + 1.5% potassium ferricyanide (BDH) in PBS (Oxoid)). The cells were resuspended during each change of solution and allowed to stand for 10 minutes, before removal of the supernatant and addition of the next processing solution. Following this, the cells were washed using several changes of distilled water to remove the osmium tetroxide and dehydrated using increasing alcohol concentrations of 30%, 50%, 70%, 90% and 100%. After dehydration, the samples were left in 50% alcohol / 50% Lemix (TAAB) epoxy resin mixture on a mixer overnight to infiltrate with resin. The samples were then placed in 100% Lemix resin for a minimum of 4 hours, embedded in fresh Lemix Resin and polymerized at 70 °C overnight. Semi-thin (1μm) sections were cut using glass knives on a Reichert-Jung Ultracut microtome, collected on glass microscope slides and stained using Toluidine Blue solution (1% Toluidine Blue (Raymond Lamb) with 0.2% Pyronin (Raymond Lamb) in 1% sodium tetraborate (Analar BDH)). Ultrathin sections were cut using a diamond knife (Diatome) and collected on 300HS, 3.05 mm copper grids (Gilder). The ultrathin sections were stained using saturated alcoholic uranyl acetate (UA) (TAAB) for 5 minutes followed by Reynold's lead citrate, also for 5 minutes. Sections examined with EDAX were not stained with UA or lead. The sections were viewed

and photographed using a Philips CM120 transmission electron microscope fitted with EDAX DX-4 microanalytical system for X-ray microanalysis of the samples.

Cell blocking experiments. Cells were pre-treated with the fucoidans or DSO4 500 at either 30 or 60 μg/mL for 15 minutes before being challenged with ferucarbotran (0.1, 0.5, 1 mgFe/mL) for 4 hours at 37°C. All experiments were performed in triplicate and repeated on three separate occasions on different days. For blocking experiments with FVF and DSO4 500 at equimolar concentrations, cells were pretreated with 0.17 μM of either blocker before adding 0.5 mgFe/mL of the SPIONs (ferucarbotran, perimag®-plain, perimag®-COOH or perimag®-NH_2) for 4 hours. Then cells were lysed and the intracellular iron content determined using ferrozine assay as described above.

In vivo experiments. All *in vivo* experiments were performed using mouse models in compliance with licenses issued under the U.K. Animals (Scientific Procedures) Act 1986 after local ethical committee review. All mice used were female Balb/c or C57BL/6 (Charles River Laboratories, UK) with an average weight of 20 g at the start of the experiments. SPIONs and fucoidans were prepared in PBS and sterile filtered (using 0.22 μm syringe filter) under a cell culture hood prior to injection, in order to minimize bacterial contamination. All injections were administered intravenously through tail veins. Fucoidans were injected at 15 mg/kg.

Radiolabeling of ferucarbotran with technetium-99m (^{99m}Tc). Technetium-99m-dipicolylamine-alendronate (^{99m}Tc-DPA-ale) linker was synthesized as previously described.[56-57] The linker was purified using a C18 Sep-Pak® light column, yielding 200 μL of 460 MBq of ^{99m}Tc-DPA-ale in dH_2O. Then 3 μL of ferucarbotran (0.174 mgFe) was added and the mixture was incubated at 40 °C for 30 minutes while shaking. The vial was then cooled to room temperature and the contents transferred to an Amicon® Ultra 0.5 mL centrifugal filter with a 10 kDa cut off that had been previously washed with 3 × 500 μL of dH_2O. The filter was

centrifuged at 11,000 x g for 3 minutes. The remaining retained solution contained 50 μL of radiolabeled nanoparticles to which 300 μL of saline was added and the mixture was sonicated for 1 minute and centrifuged as described before. This process was repeated 5 times until no more unbound ^{99}Tc-DPA-ale was detected in the filtrates. The total radioactivity in the filtrates and SPIONs solution was measured to determine the radiolabeling yield (36%). DLS performed after conjugation confirmed colloidal stability of ferucarbotran.

SPECT/CT imaging. Prior to injections and imaging, female BALB/c mice (6-8 weeks) were anesthetized with isoflurane and oxygen mixture for the duration of the experiment and sacrificed by cervical dislocation at the end of the imaging session. All injections were done intravenously through the tail vein using 0.3 mL insulin syringes. For the FVF (+) group (n = 5), mice were injected with 100 μL of FVF solution at a dose of 15 mg/kg followed by 100 μL of the ^{99}Tc-DPA-ale-ferucarbotran conjugate (1.76mgFe/kg, 15-30 MBq of ^{99m}Tc) after 2-10 minutes. For the FVF (-) group (n = 5), mice were treated with 100 μL of PBS along with 100 μL of radiolabeled ferucarbotran. Immediately after the injections the mice were imaged with SPECT/CT. SPECT/CT images were obtained with a NanoSPECT/CT PLUS preclinical animal scanner (Mediso, Hungary) equipped with four heads, each with nine 1 mm pinhole collimators, in helical scanning mode in 20 projections over 20 minutes. The CT images were obtained with a 45 kV peak X-ray source, 1000 ms exposure time in 180 projections over 10 minutes. Images were reconstructed in a 256 × 256 matrix using the HiSPECT (Scivis GmbH) reconstruction software package, and fused using InVivoScope (IVS) software (Bioscan, France). All the images were analyzed using VivoQuant^{TM} software (inviCRO, USA), which enables the co-registration of SPECT-CT images. Scale bars represent the range between the minimum (bottom) and maximum (top) image signal intensity of their respective SPECT (color) and CT (greyscale) images

Radiolabeling of ferucarbotran with zirconium-89 (^{89}Zr). Radiolabelling with ^{89}Zr was performed following a published method.[65] Zirconium-89-oxalate ($^{89}Zr^{4+}$ in 1M oxalic acid, PerkinElmer) 16 µL, 33 MBq was added to an Eppendorf tube. Chelex-treated water (200 µL) was then added and the pH raised to 8 using 1M Na_2CO_3 (aq.). This step was performed cautiously as acid neutralization with Na_2CO_3 generates CO_2 gas and base must be added carefully to avoid loss of radioactivity. Chelex-treated water was again added (200 µL), followed by the addition of ferucarbotran (52 µL, 58 mgFe/mL). The mixture was then vortexed briefly and then incubated at 100 °C for 1 h. The reaction was allowed to cool to room temperature and DTPA (50 µL, 10 mM (pH 7.5) was added and left to stir at room temperature for 30 minutes. After which time, the nanoparticle mixture was purified using size exclusion chromatography (SEC) (PD-10 Sephadex, G25) and eluted with fractions of sterile saline (recovery = 78%). ^{89}Zr-ferucarbotran was diluted to 260 µL using sterile saline. The conjugate was then characterized using dynamic light scattering (DLS) (Supplementary Table S6).

Radiolabeling of perimag®-COOH with zirconium-89 (^{89}Zr). Radiolabelling with ^{89}Zr was performed following a published method.[65] Zirconium-89-oxalate ($^{89}Zr^{4+}$ in 1M oxalic acid, PerkinElmer) 26 µL, 35.6 MBq was added to an Eppendorf tube. Chelex-treated water (200 µL) was then added and the pH raised to 8 using 1M Na_2CO_3 (aq.); base was added carefully to avoid loss of radioactivity. Chelex-treated water was again added (170 µL), followed by the addition of perimag®-COOH (20 µL, 18.2 mgFe/mL). The mixture was then vortexed briefly and incubated at 100 °C for 60 minutes. The reaction was allowed to cool to room temperature and DTPA (50 µL, 10 mM (pH 7.5)) was added and left to stir at room temperature for 30 minutes. After which time, the nanoparticle mixture was purified using size exclusion chromatography (SEC) (PD10 Sephadex, G25) and eluted with fractions of sterile saline

(recovery = 81%). ^{89}Zr-Perimag®-COOH was diluted to 260 μL using sterile saline. The conjugate was then characterized using DLS (Supplementary Table S6).

PET/CT imaging. C57BL/6 mice were injected with 100 μL ^{89}Zr-ferucarbotran or ^{89}Zr-perimag®-COOH solution (1.76 mgFe/kg), preceded by, or at the same time as, 100 μL of PBS or FVF (15 mg/kg, in PBS). At pre-set time points following injection of SPIONs, mice were anaesthetized with isoflurane (2% in oxygen) and placed on the preheated bed of the scanner (set at 38℃). Whole body static PET scans were acquired using nanoScan PET/CT (Mediso, Budapest, Hungary) followed by CT image acquisition. PET images were acquired using 1-5 coincidence mode and recorded for 20 minutes. CT images were acquired using a 50 kV peak X-ray source and 300 ms exposure time in 720 projections with an acquisition time of 7 minutes. Respiration rate was monitored throughout the scan. PET images were reconstructed using Tera-TomoTM 3D PET reconstruction software (Mediso version 2.01). CT images were reconstructed in voxel size of 68 x 68 x 68 mm using Nucline software (Mediso version 2.01). Image analysis and three-dimensional (3D) visualization were performed using VivoQuant software (InviCRO version 1.23patch3). Scale bars represent the range between the minimum (bottom) and maximum (top) image signal intensity of their respective PET (color) and CT (greyscale) images.

Subcutaneous tumor implantation in C57BL/6 mice. GL261 glioma cells were grown in filtered Dulbecco's modified Eagle's medium (DMEM) (Gibco®) supplemented with 10% fetal bovine serum (FBS) (Gibco®), and 1% sodium pyruvate until 80% confluent. Cells were detached using trypsin, and counted before being re-suspended in sterile PBS at a concentration of 5 x 10^6 cells/100 μL. Animals were anaesthetized with 2% isoflurane and 100 μL of the cell suspension was injected into the right flank. Animals were monitored closely for any adverse signs following injection. Tumor growth was monitored and animals were used for experiments

once the tumors were > 50 mm^3 in volume as measured using callipers (approximately 2-3 weeks post implantation).

Ex vivo biodistribution studies. Biodistribution studies were carried out in accordance with the British Home Office regulations governing animal experimentation. The mice from the imaging studies were used for the biodistribution studies. Mice under anesthesia were culled by cervical dislocation and the organs of interest were harvested. Each sample was weighed and counted with a gamma counter (LKB compugamma for ^{99m}Tc studies, Wizard 2480 PerkinElmer for ^{89}Zr studies), together with standards prepared from a sample of the radiolabeled SPIONs. The percent of injected dose per gram (%ID/g) of tissue was calculated for each tissue type.

Blood clearance and pharmacokinetics experiments. To assess the blood clearance and calculate pharmacokinetic data, blood samples were collected from the tail using 20 μL heparinized capillary tubes. Each sample was weighed and counted with a gamma counter (LKB compugamma for ^{99m}Tc studies, Wizard 2480 PerkinElmer for ^{89}Zr studies), together with standards prepared from a sample of the radiolabeled SPIONs. For ^{99m}Tc-ferucarbotran studies, blood samples were obtained at 3, 15, 35, 52, 67, 82, 93 and 152 minutes post injection; for ^{89}Zr-ferucarbotran, samples were taken at 5, 10, 20, 40, 60 and 180 minutes post injection; and for ^{89}Zr-perimag®-COOH studies, blood samples were obtained at 10, 20, 40, 60 and 80 minutes post SPION injection. To calculate the pharmacokinetic parameters, the %ID/g values obtained from gamma counting the blood samples were plotted against time and the data was fitted to a two-compartment model using Graphpad Prism 7 (Two phase decay non-linear regression).

ASSOCIATED CONTENT

Supplementary Data is available online on the ACS Nano website. Supplementary data includes: Experimental Section; Biological safety and dose justification of Fucus vesiculosus (FVF); *In vivo* comparison of fucoidans from different species of seaweed using NIR labelled ferucarbotran; Digital Image Analysis; Characterization of fucoidan using size exclusion chromatography-multiangle light scattering (SEC-MALS) (Wyatt Technologies UK). Supplementary Results; *In vivo* comparison of fucoidans from different species of seaweed using NIR labelled ferucarbotran; Biodistribution of ^{99m}Tc-DPA-Ale and ^{89}Zr-oxalate in C57BL/6 mice; Histological analysis of the effect of fucoidan on ferucarbotran uptake in the liver; Characterization of fucoidan using size exclusion chromatography-multiangle light scattering (SEC-MALS) (Wyatt Technologies UK); Characterization of SPIONs following technetium-99m and zirconium-89 radiolabeling using dynamic light scattering (DLS); Ex-vivo biodistribution data.

ACKNOWLEDGMENTS

The authors would like to thank Q. A. Pankhurst for helpful discussions, Meito Sangyo Co. LTD., Japan for providing ferucarbotran, Kevin Jackson (Wyatt Technology UK) for his assistance in characterizing the fucoidan samples and UCL IQPath for performing Prussian blue histology. The authors acknowledge financial support from the EU Framework 7 Programme DARTRIX project contract no. 234870, the King's College London and UCL Comprehensive Cancer Imaging Centre funded by the CRUK and EPSRC in association with the MRC and DoH (England), British Council Institutional Links grant (ID: 277386067) under the Russia-UK partnership, King's Health Partners (KHP) Research and Development Challenge Fund award (R160402), The Centre of Excellence in Medical Engineering funded by the Wellcome Trust and EPSRC under Grant No. WT 088641/Z/09/Z, Department of Health *via* the National Institute for Health Research (NIHR) Biomedical Research Centre based at Guy's & St Thomas' NHS Foundation Trust and King's College London, Celia Abrahams and the Mothers and Daughters Committee, the National Brain Appeal, Cancer Research UK (CR-UK), Department of Health (ECMC, Experimental Cancer Medicine Network Centre), NIHR University College London Hospitals Biomedical Research Centre and Cancer Research UK Accelerator Grant (Cl 15121 A 20256). The views expressed are those of the authors and not necessarily those of the NHS, NIHR or the Department of Health.

REFERENCES

1. Rosen, J. E.; Chan, L.; Shieh, D.-B.; Gu, F. X., Iron Oxide Nanoparticles for Targeted Cancer Imaging and Diagnostics. *Nanomed. Nanotech. Biol. Med.* **2012,** *8*, 275-290.

2. Weissig, V.; Pettinger, T. K.; Murdock, N., Nanopharmaceuticals (Part 1): Products on the Market. *Int. J. Nanomed.* **2014,** *9*, 4357.

3. Lu, M.; Cohen, M. H.; Rieves, D.; Pazdur, R., FDA report: Ferumoxytol for Intravenous Iron Therapy in Adult Patients with Chronic Kidney Disease. *Am. J. Hematol.* **2010,** *85*, 315-319.

4. Tassa, C.; Shaw, S. Y.; Weissleder, R., Dextran-Coated Iron Oxide Nanoparticles: A Versatile Platform for Targeted Molecular Imaging, Molecular Diagnostics, and Therapy. *Acc. Chem. Res.* **2011,** *44*, 842-852.

5. Mallory, M.; Gogineni, E.; Jones, G. C.; Greer, L.; Simone, C. B., Therapeutic Hyperthermia: The Old, the New, and the Upcoming. *Crit. Rev. in Oncol. Hematol.* **2015**, *97*, 55-64

6. Panagiotopoulos, N.; Duschka, R. L.; Ahlborg, M.; Bringout, G.; Debbeler, C.; Graeser, M.; Kaethner, C.; Lüdtke-Buzug, K.; Medimagh, H.; Stelzner, J.; Buzug, T. M.; Barkhausen, J.; Vogt, F. M.; Haegele, J., Magnetic Particle Imaging: Current Developments and Future Directions. *Int. J. Nanomed.* **2015,** *10*, 3097-3114.

7. Grootendorst, D. J.; Jose, J.; Fratila, R. M.; Visscher, M.; Velders, A. H.; Ten Haken, B.; Van Leeuwen, T. G.; Steenbergen, W.; Manohar, S.; Ruers, T. J., Evaluation of Superparamagnetic Iron Oxide Nanoparticles (Endorem®) as a Photoacoustic Contrast Agent for Intra-Operative Nodal Staging. *Contrast Media Mol Imaging* **2013,** *8*, 83-91.

8. Weissleder, R.; Nahrendorf, M.; Pittet, M. J., Imaging Macrophages with Nanoparticles. *Nat. Mater.* **2014,** *13*, 125-138.

9. Tang, T. Y.; Howarth, S. P.; Miller, S. R.; Graves, M. J.; Patterson, A. J.; JM, U. K.-I.; Li, Z. Y.; Walsh, S. R.; Brown, A. P.; Kirkpatrick, P. J.; Warburton, E. A.; Hayes, P. D.; Varty, K.; Boyle, J. R.; Gaunt, M. E.; Zalewski, A.; Gillard, J. H., The ATHEROMA (Atorvastatin Therapy: Effects on Reduction of Macrophage Activity) Study. Evaluation Using Ultrasmall Superparamagnetic Iron Oxide-Enhanced Magnetic Resonance Imaging in Carotid Disease. *J. Am. Coll. Cardiol.* **2009,** *53*, 2039-50.

10. Kooi, M.; Cappendijk, V.; Cleutjens, K.; Kessels, A.; Kitslaar, P.; Borgers, M.; Frederik, P.; Daemen, M.; Van Engelshoven, J., Accumulation of Ultrasmall Superparamagnetic Particles of Iron Oxide in Human Atherosclerotic Plaques Can Be Detected by *in Vivo* Magnetic Resonance Imaging. *Circulation* **2003,** *107*, 2453-2458.

11. Richards, J. M.; Semple, S. I.; MacGillivray, T. J.; Gray, C.; Langrish, J. P.; Williams, M.; Dweck, M.; Wallace, W.; McKillop, G.; Chalmers, R. T., Abdominal Aortic Aneurysm Growth Predicted by Uptake of Ultrasmall Superparamagnetic Particles of Iron Oxide a Pilot Study. *Circ. Cardiovasc. Imaging* **2011,** *4*, 274-281.

12. Gaglia, J. L.; Harisinghani, M.; Aganj, I.; Wojtkiewicz, G. R.; Hedgire, S.; Benoist, C.; Mathis, D.; Weissleder, R., Noninvasive Mapping of Pancreatic Inflammation in Recent-Onset Type-1 Diabetes Patients. *Proc. Natl. Acad. Sci.* **2015,** *112*, 2139-2144.

13. Xu, X.; Ho, W.; Zhang, X.; Bertrand, N.; Farokhzad, O., Cancer Nanomedicine: From Targeted Delivery to Combination Therapy. *Trends Mol. Med.* **2015,** *21*, 223-232.

14. Gaur, U.; Sahoo, S. K.; De Tapas, K.; Ghosh, P. C.; Maitra, A.; Ghosh, P., Biodistribution of Fluoresceinated Dextran Using Novel Nanoparticles Evading Reticuloendothelial System. *Int. J. Pharm.* **2000,** *202*, 1-10.

15. Shubayev, V. I.; Pisanic, T. R.; Jin, S., Magnetic Nanoparticles for Theragnostics. *Adv. Drug Deliv. Rev.* **2009,** *61*, 467-477.

16. Gupta, A. K.; Gupta, M., Synthesis and Surface Engineering of Iron Oxide Nanoparticles for Biomedical Applications. *Biomaterials* **2005,** *26*, 3995-4021.

17. Fan, C.; Gao, W.; Chen, Z.; Fan, H.; Li, M.; Deng, F.; Chen, Z., Tumor Selectivity of Stealth Multi-Functionalized Superparamagnetic Iron Oxide Nanoparticles. *Int, J. Pharm.* **2011,** *404*, 180-190.

18. Gabizon, A. A., Stealth Liposomes and Tumor Targeting: One Step Further in the Quest for the Magic Bullet. *Clin. Cancer Res.* **2001,** *7*, 223-225.

19. Leckband, D.; Israelachvili, J., Intermolecular Forces in Biology. *Q. Rev. Biophys.* **2001,** *34*, 105-267.

20. Li, S.-D.; Huang, L., Stealth Nanoparticles: High Density but Sheddable PEG is a Key for Tumor Targeting. *J. Control. Release* **2010,** *145*, 178.

21. Moghimi, S. M.; Szebeni, J., Stealth Liposomes and Long Circulating Nanoparticles: Critical Issues in Pharmacokinetics, Opsonization and Protein-Binding Properties. *Prog. Lipid Res.* **2003,** *42*, 463-478.

22. Blanco, E.; Shen, H.; Ferrari, M., Principles of Nanoparticle Design for Overcoming Biological Barriers to Drug Delivery. *Nat. Biotechnol.* **2015,** *33*, 941-951.

23. Gao, Z.; Zhang, L.; Hu, J.; Sun, Y., Mesenchymal Stem Cells: A Potential Targeted-Delivery Vehicle for Anti-Cancer Drug Loaded Nanoparticles. *Nanomed. Nanotech. Biol. Med.* **2013,** *9*, 174-184.

24. Rodriguez, P. L.; Harada, T.; Christian, D. A.; Pantano, D. A.; Tsai, R. K.; Discher, D. E., Minimal" Self" Peptides That Inhibit Phagocytic Clearance and Enhance Delivery of Nanoparticles. *Science* **2013,** *339*, 971-975.

25. Parodi, A.; Quattrocchi, N.; van de Ven, A. L.; Chiappini, C.; Evangelopoulos, M.; Martinez, J. O.; Brown, B. S.; Khaled, S. Z.; Yazdi, I. K.; Enzo, M. V., Synthetic Nanoparticles Functionalized with Biomimetic Leukocyte Membranes Possess Cell-Like Functions. *Nat. Nanotechnol.* **2013,** *8*, 61-68.

26. Hu, C.-M. J.; Fang, R. H.; Wang, K.-C.; Luk, B. T.; Thamphiwatana, S.; Dehaini, D.; Nguyen, P.; Angsantikul, P.; Wen, C. H.; Kroll, A. V.; Carpenter, C.; Ramesh, M.; Qu, V.; Patel, S. H.; Zhu, J.; Shi, W.; Hofman, F. M.; Chen, T. C.; Gao, W.; Zhang, K.; Chien, S.; Zhang, L., Nanoparticle Biointerfacing by Platelet Membrane Cloaking. *Nature* **2015,** *526*, 118-121.

27. Hu, C.-M. J.; Zhang, L.; Aryal, S.; Cheung, C.; Fang, R. H.; Zhang, L., Erythrocyte Membrane-Camouflaged Polymeric Nanoparticles as a Biomimetic Delivery Platform. *Proc. Natl. Acad. Sci.* **2011,** *108*, 10980-10985.

28. Antonelli, A.; Sfara, C.; Battistelli, S.; Canonico, B.; Arcangeletti, M.; Manuali, E.; Salamida, S.; Papa, S.; Magnani, M., New Strategies to Prolong the *in Vivo* Life Span of Iron-Based Contrast Agents for MRI. *PloS One* **2013,** *8*, e78542.

29. Khalid, A.; Persano, S.; Shen, H.; Zhao, Y.; Blanco, E.; Ferrari, M.; Wolfram, J., Strategies for Improving Drug Delivery: Nanocarriers and Microenvironmental Priming. *Expert Opin. Drug Deliv.* **2017,** *14*, 865-877.

30. Abdollah, M. R.; Kalber, T.; Tolner, B.; Southern, P.; Bear, J. C.; Robson, M.; Pedley, R. B.; Parkin, I. P.; Pankhurst, Q. A.; Mulholland, P.; Chester, K., Prolonging the Circulatory Retention of SPIONs Using Dextran Sulfate: *In Vivo* Tracking Achieved by Functionalisation with Near-Infrared Dyes. *Faraday Discuss.* **2014,** *175*, 41-58

31. Reimer, P.; Balzer, T., Ferucarbotran (Resovist): A New Clinically Approved RES-Specific Contrast Agent for Contrast-Enhanced MRI of the Liver: Properties, Clinical Development, and Applications. *Eur. Radiol.* **2003,** *13*, 1266-1276.

32. Flexner, C.; Barditch-Crovo, P. A.; Kornhauser, D. M.; Farzadegan, H.; Nerhood, L. J.; Chaisson, R. E.; Bell, K. M.; Lorentsen, K. J.; Hendrix, C. W.; Petty, B. G., Pharmacokinetics, Toxicity, and Activity of Intravenous Dextran Sulfate in Human Immunodeficiency Virus Infection. *Antimicrob. Agents Chemother.* **1991,** *35*, 2544.

33. Thelen, T.; Hao, Y.; Medeiros, A. I.; Curtis, J. L.; Serezani, C. H.; Kobzik, L.; Harris, L. H.; Aronoff, D. M., The Class A Scavenger Receptor, Macrophage Receptor with Collagenous Structure, is the Major Phagocytic Receptor for Clostridium Sordellii Expressed by Human Decidual Macrophages. *Journal Immunol.* **2010,** *185*, 4328-4335.

34. Raynal, I.; Prigent, P.; Peyramaure, S.; Najid, A.; Rebuzzi, C.; Corot, C., Macrophage Endocytosis of Superparamagnetic Iron Oxide Nanoparticles: Mechanisms and Comparison of Ferumoxides and Ferumoxtran-10. *Invest. Radiol.* **2004,** *39*, 56.

35. Lunov, O.; Zablotskii, V.; Syrovets, T.; Röcker, C.; Tron, K.; Nienhaus, G. U.; Simmet, T., Modeling Receptor-Mediated Endocytosis of Polymer-Functionalized Iron Oxide Nanoparticles by Human Macrophages. *Biomaterials* **2010**, 547-555

36. Yang, C. Y.; Tai, M. F.; Lin, C. P.; Lu, C. W.; Wang, J. L.; Hsiao, J. K.; Liu, H. M., Mechanism of Cellular Uptake and Impact of Ferucarbotran on Macrophage Physiology. *PloS One* **2011,** *6*, e25524.

37. Chao, Y.; Karmali, P. P.; Simberg, D., Role of Carbohydrate Receptors in the Macrophage Uptake of Dextran-Coated Iron Oxide Nanoparticles. *Nano-Biotechnology for Biomedical and Diagnostic Research* **2012**, 115-123.

38. Chao, Y.; Makale, M.; Karmali, P. P.; Sharikov, Y.; Tsigelny, I.; Merkulov, S.; Kesari, S.; Wrasidlo, W.; Ruoslahti, E.; Simberg, D., Recognition of Dextran–Superparamagnetic Iron Oxide Nanoparticle Conjugates (Feridex) *via* Macrophage Scavenger Receptor Charged Domains. *Bioconjug. Chem.* **2012,** *23*, 1003-1009.

39. Li, B.; Lu, F.; Wei, X.; Zhao, R., Fucoidan: Structure and Bioactivity. *Molecules* **2008,** *13*, 1671-1695.

40. Cumashi, A.; Ushakova, N. A.; Preobrazhenskaya, M. E.; D'incecco, A.; Piccoli, A.; Totani, L.; Tinari, N.; Morozevich, G. E.; Berman, A. E.; Bilan, M. I., A Comparative Study of the Anti-Inflammatory, Anticoagulant, Antiangiogenic, and Antiadhesive Activities of Nine Different Fucoidans from Brown Seaweeds. *Glycobiology* **2007,** *17*, 541-552.

41. Fitton, J. H., Therapies from Fucoidan; Multifunctional Marine Polymers. *Mar. Drugs* **2011,** *9*, 1731-1760.

42. Lira, M.; Santos-Magalhães, N.; Nicolas, V.; Marsaud, V.; Silva, M.; Ponchel, G.; Vauthier, C., Cytotoxicity and Cellular Uptake of Newly Synthesized Fucoidan-Coated Nanoparticles. *Eur. J. Pharm. Biopharm.* **2011,** *79*, 162-170.

43. Kwak, J.-Y., Fucoidan as a Marine Anticancer Agent in Preclinical Development. *Mar. Drugs* **2014,** *12*, 851-870.

44. Raschke, W.; Baird, S.; Ralph, P.; Nakoinz, I., Functional Macrophage Cell Lines Transformed by Abelson Leukemia Virus. *Cell* **1978,** *15*, 261-267.

45. Lunov, O.; Syrovets, T.; Röcker, C.; Tron, K.; Ulrich Nienhaus, G.; Rasche, V.; Mailänder, V.; Landfester, K.; Simmet, T., Lysosomal Degradation of the Carboxydextran Shell of Coated Superparamagnetic Iron Oxide Nanoparticles and the Fate of Professional Phagocytes. *Biomaterials* **2010,** *31*, 9015-9022.

46. Riemer, J.; Hoepken, H. H.; Czerwinska, H.; Robinson, S. R.; Dringen, R., Colorimetric Ferrozine-Based Assay for the Quantitation of Iron in Cultured Cells. *Anal. Biochem.* **2004,** *331*, 370-375.

47. Kalber, T. L.; Smith, C. J.; Howe, F. A.; Griffiths, J. R.; Ryan, A. J.; Waterton, J. C.; Robinson, S. P., A Longitudinal Study of R2* and R2 Magnetic Resonance Imaging Relaxation Rate Measurements in Murine Liver After a Single Administration of 3 Different Iron Oxide-Based Contrast Agents. *Invest. Radiol.* **2005,** *40*, 784.

48. Schöpf, B.; Neuberger, T.; Schulze, K.; Petri, A.; Chastellain, M.; Hofmann, M.; Hofmann, H.; Von Rechenberg, B., Methodology Description for Detection of Cellular Uptake of PVA Coated Superparamagnetic Iron Oxide Nanoparticles (SPION) in Synovial Cells of Sheep. *J. Magn. Magn. Mater.* **2005,** *293*, 411-418.

49. Smith, B. R.; Heverhagen, J.; Knopp, M.; Schmalbrock, P.; Shapiro, J.; Shiomi, M.; Moldovan, N. I.; Ferrari, M.; Lee, S. C., Localization to Atherosclerotic Plaque and Biodistribution of Biochemically Derivatized Superparamagnetic Iron Oxide Nanoparticles (SPIONs) Contrast Particles for Magnetic Resonance Imaging (MRI). *Biomed. Microdevices* **2007,** *9*, 719-727.

50. Lee, J. H.; Smith, M. A.; Liu, W.; Gold, E. M.; Lewis, B.; Song, H. T.; Frank, J. A., Enhanced Stem Cell Tracking *via* Electrostatically Assembled Fluorescent SPION–Peptide Complexes. *Nanotechnology* **2009,** *20*, 355102.

51. Branca, R. T.; Cleveland, Z. I.; Fubara, B.; Kumar, C. S. S. R.; Maronpot, R. R.; Leuschner, C.; Warren, W. S.; Driehuys, B., Molecular MRI for Sensitive and Specific Detection of Lung Metastases. *Proc. Natl. Acad. Sci.* **2010,** *107*, 3693.

52. Hsiao, J. K.; Chu, H. H.; Wang, Y. H.; Lai, C. W.; Chou, P. T.; Hsieh, S. T.; Wang, J. L.; Liu, H. M., Macrophage Physiological Function After Superparamagnetic Iron Oxide Labeling. *NMR in Biomedicine* **2008,** *21*, 820-829.

53. Sonia, S.; Mirko, M.; Chiara, F.; Marina, P.; Federica, B.; Umberto, B.; Marco, G., Ascorbic Acid Pre-Treated Quartz Stimulates TNF-α Release in RAW 264.7 Murine Macrophages Through ROS Production and Membrane Lipid Peroxidation. *Respir. Res.* **2009,** *10*, 25

54. Segers, F. M.; den Adel, B.; Bot, I.; van der Graaf, L. M.; van der Veer, E. P.; Gonzalez, W.; Raynal, I.; de Winther, M.; Wodzig, W. K.; Poelmann, R. E., Scavenger Receptor-AI–Targeted Iron Oxide Nanoparticles for *in Vivo* MRI Detection of Atherosclerotic Lesions. *Arterioscler. Thromb. Vasc. Biol.* **2013,** *33*, 1812-1819.

55. Sandiford, L.; Phinikaridou, A.; Protti, A.; Meszaros, L. K.; Cui, X.; Yan, Y.; Frodsham, G.; Williamson, P. A.; Gaddum, N.; Botnar, R. M., Bisphosphonate-Anchored PEGylation and Radiolabeling of Superparamagnetic Iron Oxide: Long-Circulating Nanoparticles for *in Vivo* Multimodal (T1 MRI-SPECT) Imaging. *ACS Nano* **2012,** *7*, 500-512.

56. de Rosales, R. T. M.; Tavaré, R.; Glaria, A.; Varma, G.; Protti, A.; Blower, P. J., 99mTc-Bisphosphonate-Iron Oxide Nanoparticle Conjugates for Dual-Modality Biomedical Imaging. *Bioconjug. Chem.* **2011,** *22*, 455-465.

57. De Rosales, R. T. M.; Finucane, C.; Mather, S.; Blower, P., Bifunctional Bisphosphonate Complexes for the Diagnosis and Therapy of Bone Metastases. *Chem. Commun.* **2009,** 32, 4847-4849.

58. Ahmed, M.; de Rosales, R. T. M.; Douek, M., Preclinical Studies of the Role of Iron Oxide Magnetic Nanoparticles for Nonpalpable Lesion Localization in Breast Cancer. *J. Surg. Res.* **2013,** *185*, 27-35.

59. Wang, J. T. W.; Cabana, L.; Bourgognon, M.; Kafa, H.; Protti, A.; Venner, K.; Shah, A. M.; Sosabowski, J. K.; Mather, S. J.; Roig, A., Magnetically Decorated Multiwalled Carbon Nanotubes as Dual MRI and SPECT Contrast Agents. *Adv. Funct. Mater.* **2014,** *24*, 1880-1894.

60. Jedlovszky-Hajdú, A. l.; Bombelli, F. B.; Monopoli, M. P.; Tombácz, E.; Dawson, K. A., Surface Coatings Shape the Protein Corona of SPIONs with Relevance to Their Application *in Vivo*. *Langmuir* **2012,** *28*, 14983-14991.

61. Sakulkhu, U.; Mahmoudi, M.; Maurizi, L.; Salaklang, J.; Hofmann, H., Protein Corona Composition of Superparamagnetic Iron Oxide Nanoparticles with Various Physico-Chemical Properties and Coatings. *Sci. Rep.* **2014,** *4*.

62. Inturi, S.; Wang, G.; Chen, F.; Banda, N. K.; Holers, V. M.; Wu, L.; Moghimi, S. M.; Simberg, D., Modulatory Role of Surface Coating of Superparamagnetic Iron Oxide

Nanoworms in Complement Opsonization and Leukocyte Uptake. *ACS Nano* **2015,** *9*, 10758-10768.

63. Chen, F.; Wang, G.; Griffin, J. I.; Brenneman, B.; Banda, N. K.; Holers, V. M.; Backos, D. S.; Wu, L.; Moghimi, S. M.; Simberg, D., Complement Proteins Bind to Nanoparticle Protein Corona and Undergo Dynamic Exchange *in Vivo*. *Nat. Nanotechnol.* **2017,** *12*, 387-393.

64. Simberg, D., Iron Oxide Nanoparticles and the Mechanisms of Immune Recognition of Nanomedicines. Future Medicine. **2016**, 741-743

65. Boros, E.; Bowen, A. M.; Josephson, L.; Vasdev, N.; Holland, J. P., Chelate-Free Metal Ion Binding and Heat-Induced Radiolabeling of Iron Oxide Nanoparticles. *Chem. Sci.* **2015,** *6*, 225-236.

66. Chouly, C.; Pouliquen, D.; Lucet, I.; Jeune, J.; Jallet, P., Development of Superparamagnetic Nanoparticles for MRI: Effect of Particle Size, Charge and Surface Nature on Biodistribution. *J. Microencapsul.* **1996,** *13*, 245-255.

67. Szatmári, T.; Lumniczky, K.; Désaknai, S.; Trajcevski, S.; Hídvégi, E. J.; Hamada, H.; Sáfrány, G., Detailed Characterization of the Mouse Glioma 261 Tumor Model for Experimental Glioblastoma Therapy. *Cancer Sci.* **2006,** *97*, 546-553.

68. Reardon, D. A.; Gokhale, P. C.; Klein, S. R.; Ligon, K. L.; Rodig, S. J.; Ramkissoon, S. H.; Jones, K. L.; Conway, A. S.; Liao, X.; Zhou, J., Glioblastoma Eradication Following Immune Checkpoint Blockade in an Orthotopic, Immunocompetent Model. *Cancer Immunol. Res.* **2016,** *4*, 124-135.

69. Wainwright, D. A.; Chang, A. L.; Dey, M.; Balyasnikova, I. V.; Kim, C. K.; Tobias, A.; Cheng, Y.; Kim, J. W.; Qiao, J.; Zhang, L., Durable Therapeutic Efficacy Utilizing Combinatorial Blockade Against IDO, CTLA-4, and PD-L1 in Mice with Brain Tumors. *Clin. Cancer Res.* **2014,** *20*, 5290-5301.

70. Mantovani, A.; Marchesi, F.; Malesci, A.; Laghi, L.; Allavena, P., Tumour-Associated Macrophages as Treatment Targets in Oncology. *Nat. Rev. Clin. Oncol.* **2017**.

71. Zanganeh, S.; Hutter, G.; Spitler, R.; Lenkov, O.; Mahmoudi, M.; Shaw, A.; Pajarinen, J. S.; Nejadnik, H.; Goodman, S.; Moseley, M., Iron Oxide Nanoparticles Inhibit Tumour Growth by Inducing Pro-Inflammatory Macrophage Polarization in Tumour Tissues. *Nat. Nanotechnol.* **2016,** *11*, 986-994.

72. Rojas, J. M.; Sanz-Ortega, L.; Mulens-Arias, V.; Gutiérrez, L.; Pérez-Yagüe, S.; Barber, D. F., Superparamagnetic Iron Oxide Nanoparticle Uptake Alters M2 Macrophage Phenotype, Iron Metabolism, Migration and Invasion. *Nanomed. Nanotech. Biol. Med.* **2016,** *12* (4), 1127-1138.

73. Neyen, C.; Plüddemann, A.; Mukhopadhyay, S.; Maniati, E.; Bossard, M.; Gordon, S.; Hagemann, T., Macrophage Scavenger Receptor A Promotes Tumor Progression in Murine Models of Ovarian and Pancreatic Cancer. *J. Immunol* **2013,** *190*, 3798-3805.

74. Kim, M.-H.; Joo, H.-G., Immunostimulatory Effects of Fucoidan on Bone Marrow-Derived Dendritic Cells. *Immunol. Lett.* **2008,** *115*, 138-143.

75. Yang, M.; Ma, C.; Sun, J.; Shao, Q.; Gao, W.; Zhang, Y.; Li, Z.; Xie, Q.; Dong, Z.; Qu, X., Fucoidan Stimulation Induces a Functional Maturation of Human Monocyte-Derived Dendritic Cells. *Int. Immunopharmacol.* **2008,** *8*, 1754-1760.

76. Jin, J.-O.; Park, H.-Y.; Xu, Q.; Park, J.-I.; Zvyagintseva, T.; Stonik, V. A.; Kwak, J.-Y., Ligand of Scavenger Receptor Class A Indirectly Induces Maturation of Human Blood Dendritic Cells *via* Production of Tumor Necrosis Factor-α. *Blood* **2009,** *113*, 5839-5847.

77. Hu, Y.; Cheng, S. C.-S.; Chan, K.-T.; Ke, Y.; Xue, B.; Sin, F. W.-Y.; Zeng, C.; Xie, Y., Fucoidin Enhances Dendritic Cell-Mediated T-Cell Cytotoxicity Against NY-ESO-1 Expressing Human Cancer Cells. *Biochem. Biophys. Res. Commun.* **2010,** *392*, 329-334.

78. Ale, M. T.; Maruyama, H.; Tamauchi, H.; Mikkelsen, J. D.; Meyer, A. S., Fucoidan From *Sargassum Sp.* and *Fucus Vesiculosus* Reduces Cell Viability of Lung Carcinoma and Melanoma Cells *in Vitro* and Activates Natural Killer Cells in Mice *in Vivo*. *Int. J. Biol. Macromol.* **2011,** *49*, 331-336.

79. Azuma, K.; Ishihara, T.; Nakamoto, H.; Amaha, T.; Osaki, T.; Tsuka, T.; Imagawa, T.; Minami, S.; Takashima, O.; Ifuku, S., Effects of Oral Administration of Fucoidan Extracted From Cladosiphon Okamuranus on Tumor Growth and Survival Time in a Tumor-Bearing Mouse Model. *Mar. drugs* **2012,** *10*, 2337-2348.

80. Zheng, B.; Marc, P.; Yu, E.; Gunel, B.; Lu, K.; Vazin, T.; Schaffer, D. V.; Goodwill, P. W.; Conolly, S. M., Quantitative Magnetic Particle Imaging Monitors the Transplantation, Biodistribution, and Clearance of Stem Cells *in Vivo*. *Theranostics* **2016,** *6*, 291.

81. Kilian, T.; Fidler, F.; Kasten, A.; Nietzer, S.; Landgraf, V.; Weiß, K.; Walles, H.; Westphal, F.; Hackenberg, S.; Grüttner, C., Stem Cell Labeling with Iron Oxide Nanoparticles: Impact of 3D Culture on Cell Labeling Maintenance. *Nanomedicine* **2016,** *11*, 1957-1970.

82. Fröhlich, E., The Role of Surface Charge in Cellular Uptake and Cytotoxicity of Medical Nanoparticles. *Int. J. Nanomedicine* **2012,** *7*, 5577.

83. Shang, L.; Nienhaus, K.; Nienhaus, G. U., Engineered Nanoparticles Interacting with Cells: Size Matters. *J. Nanobiotechnol.* **2014,** *12*, 5.

84. Mahmoudi, M.; Laurent, S.; Shokrgozar, M. A.; Hosseinkhani, M., Toxicity Evaluations of Superparamagnetic Iron Oxide Nanoparticles: Cell "Vision" *Versus* Physicochemical Properties of Nanoparticles. *ACS Nano* **2011,** *5*, 7263-7276.

85. Wilhelm, S.; Tavares, A. J.; Dai, Q.; Ohta, S.; Audet, J.; Dvorak, H. F.; Chan, W. C., Analysis of Nanoparticle Delivery to Tumours. *Nat. Rev. Mater.* **2016,** *1*, 16014.

86. Torrice, M., Does Nanomedicine Have a Delivery Problem? *ACS Cent. Sci.* **2016,** *2*, 434.

87. Ferrari, M., Frontiers in Cancer Nanomedicine: Directing Mass Transport Through Biological Barriers. *Trends Biotechnol.* **2010,** *28*, 181-188.

88. Albanese, A.; Tang, P. S.; Chan, W. C. W., The Effect of Nanoparticle Size, Shape, and Surface Chemistry on Biological Systems. *Annu. Rev. Biomed. Eng.* **2012,** *14*, 1-16.